UNIVERSITÀ DEGLI STUDI DI NAPOLI
FEDERICO II

UNIVERSITÀ DEGLI STUDI DI NAPOLI FEDERICO II

PH.D. THESIS

IN

INFORMATION TECHNOLOGY AND ELECTRICAL ENGINEERING

SAW-LESS DIGITALLY-ASSISTED RECEIVERS

Gerardo Castellano

Tutor

Prof. Davide De Caro

Coordinator

Prof. Daniele Riccio

XXX CYCLE

SCUOLA POLITECNICA E DELLE SCIENZE DI BASE

DIPARTIMENTO DI INGEGNERIA ELETTRICA E TECNOLOGIE DELL'INFORMAZIONE

Università degli Studi di Napoli Federico II

Dipartimento di Ingegneria Elettrica e Tecnologie dell'Informazione

Doctor of Philosophy

SAW-LESS DIGITALLY-ASSISTED RECEIVERS

by Gerardo Castellano

Abstract

Today's wireless devices, like our smartphones, are able to handle multiple standards and bands for different applications, such as Bluetooth, Wi-Fi and data-voice communications. However, the cost of a modern transceiver is becoming mainly dominated by the large number of off-chip passive components, like Duplexers and SAW filters, needed to distinguish the desired signal among many interferences. Addressing the challenges that arise from the lack of RF filtering, a SAW-less architecture represents an interesting solution to reduce the platform complexity. This thesis proposes a feasible solution based on a SAW-less RF front-end able to meet the standard requirements and a digital system tailored to the RF path. The digital architecture, which represents the main topic of this thesis, is described in detail and experimentally tested to validate the proposed solutions.

Table of Contents

List of Figures

List of Tables

Chapter 1

SAW-less Multi-standard Multi-band Transceivers

In the last years high performance handset devices, like our smartphones, have showed an ever growing complexity: they need to cover many standards and frequency bands for different applications, and have to ensure high data rate wireless connectivity. In order to meet the requirements defined by standard protocols, the transceivers used in these devices need a huge number of off-chip components, among which Surface Acoustic Wave (SAW) and Duplexer filters. However, towards advanced standards (e.g. 5G), their size and cost are destined to exponentially increase to a point that cannot be accepted. For this reason, the research is pushing to find alternative solutions in order to reduce as much as possible the number of these external components. In this first chapter, a brief description of a modern Multi-standard platform is reported in Section 1.1, the challenges to be faced removing the external SAW filters are explained in Section 1.2, and finally the proposed SAW-less digitally-assisted architecture is introduced in Section 1.3.

1.1 Transceiver Architecture in Wireless Devices

Nowadays modern mobile devices have to manage different standards and modes of operations (e.g. 2G, 3G, 4G, Wi-Fi, Bluetooth, NFC, etc.) in order to meet the needs of users: fast data transfer, battery-life saving and territory coverage. Moreover, the ever growing demand for performance and higher data rate are leading to larger bandwidth (tens of MHz) and the adoption of advanced methods, like Carrier

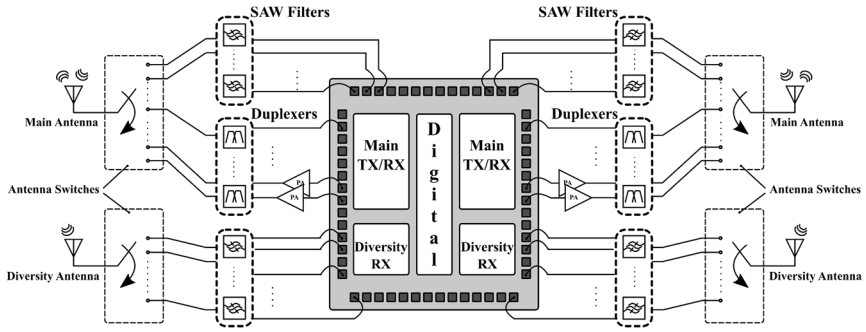

Figure 1.1: Modern Multi-standard Platform

Aggregation to combine different channels and Multiple-Input-Multiple-Output (MIMO) structures (8 paths in downlink and 4 in uplink are already implemented) to improve the capacity and the quality of the communication channels. The coexistence of multiple standards and frequency bands, and the continuous evolution towards higher performance are increasing the complexity of wireless platforms (Fig. 1.1), making challenging their realization at low cost. Although the technology scaling allows to keep low the cost of the integrated components, especially the digital circuits, the passive external elements have been only marginally interested by the technology evolution. The multiple operating bands and standards to be supported and the massive adoption of MIMO structures require a large number of external passive components, compromising the form factor of the transceiver. In particular, SAW and Duplexer filters are Radio Frequency (RF) components used to filter out-of-band signals in order to meet the standard specifications and to relax the linearity requirements of the receivers, protecting their sensitivity from self-interferences by local transmitters and from external undesired signals. These highly selective band pass filters are used between the antenna and the receiver (Rx) path to select the desired signal, and at the output of the transmitter (Tx) to reduce the RF power emissions (noise and tones) outside the Tx band. In Frequency Division Duplexing (FDD) standards, like UMTS (3G) and LTE (4G), Tx and Rx work in full duplex mode (the transmitter and receiver operate at the same time but on different frequency bands), making essential the use of an external

SAW-based duplexer. The number of RF filters are drastically increasing as the number of standards, bands and parallel Rx and Tx paths supported by the transceiver. However, these electromechanical devices, designed on piezoelectric crystal or ceramic material, have many drawbacks: lack of tunability, high cost, and bulky structure. Therefore, to keep cost, area and complexity of a modern multi-standard platform to an affordable level, it is highly desirable looking for alternative SAW-less architectures, addressing the challenges that arise from the lack of RF filtering in front of the receiver chain.

1.2 Challenges in SAW-less Receiver

In order to be used in a realistic application, a wireless receiver must verify the requirements expected by the standard. However, without any external filtering (Fig. 1.2), at the input of the receiver chain will be the desired weak signal among huge unfiltered ones, generated by

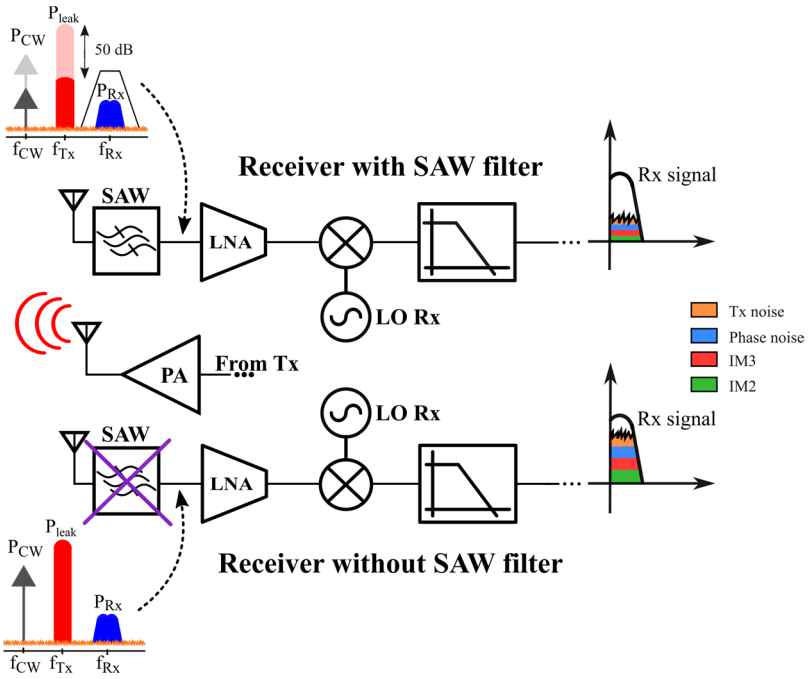

Figure 1.2: SAW-less challenges

the local transmitters and external interferences. In this situation, all the classical problems that characterize a RF receiver will be exacerbated: dynamic range, sensitivity, gain compression, reciprocal and harmonic mixing, intermodulation products, transmitter noise leakage. In this section a few basic concepts [1] will be given, with the aim of helping the comprehension of the challenges that need to be faced in a SAW-less receiver design.

1.2.1 Dynamic Range: Gain Compression and Sensitivity

The dynamic range summarizes the performance of the receiver (Fig. 1.3): it is defined as the ratio between the maximum and the minimum signal power that the receiver can properly handle. The sensitivity fixes the minimum signal that the receiver can detect with the required signal-to-noise (SNR) level, which depends on the adopted signal modulation technique and the maximum tolerated bit-error-rate (BER). The receiver sensitivity is defined as

$$S_{dB} = 10\log(K_B T_0) + 10\log(B) + NF + SNR_{\min} \qquad (1.1)$$

where K_B is the Boltzmann constant, T_0 is the temperature in Kelvin, B is the signal bandwidth in Hz, NF is the receiver noise figure and SNR_{min} is the minimum required SNR. The first term is the *available noise*

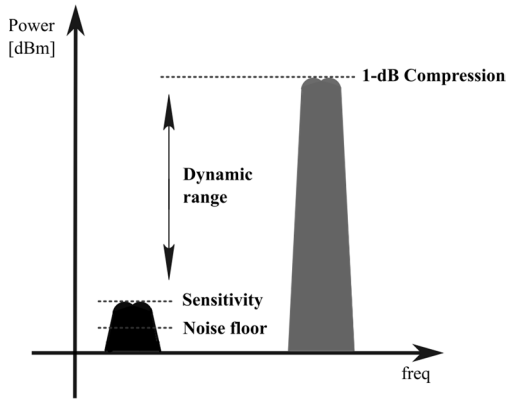

Figure 1.3: Dynamic range definition

power and, when the receiver is matched to the antenna and T_0 = 300K, is equal to -174 dBm/Hz; the sum of the first three terms of the equation (1.1) determines the "noise floor" (i.e. the total integrated noise) of the system. In particular, the noise figure is defined as the input/output SNR degradation introduced by the receiver, which depends on the noise generated by the circuit itself. The specifications imposed by the standard, namely signal bandwidth and SNR_{min}, determine an upper bound on the noise figure of the receiver. Regarding the maximum signal level that a receiver can tolerate, it is necessary to introduce the nonlinear behavior of the RF circuits. Usually, when small signals are considered, an analog circuit is approximated by an ideal linear model. However, a more realistic model of the analog circuit has to take into account the nonlinear behavior of the devices: the input/output characteristic in time domain can be approximatively expressed as

$$y(t) \approx a_1 x(t) + a_2 x^2(t) + a_3 x^3(t) \tag{1.2}$$

where a_1 is the small-signal gain of the receiver. Assuming a sinusoidal input, the output will be

$$x(t) = A\cos(\omega_0 t)$$

$$y(t) = \frac{a_2 A^2}{2} + \left(a_1 + \frac{3a_3 A^3}{4} \right)\cos(\omega_0 t) + \frac{a_2 A^2}{2}\cos(2\omega_0 t) + \frac{a_3 A^3}{4}\cos(3\omega_0 t) \tag{1.3}$$

The harmonic distortion generates at the system output not only a signal at the fundamental frequency ω_0 but also components at integer multiples of the input frequency. The gain at the fundamental frequency is a function of both linear a_1 and nonlinear a_3 coefficients, and it also depends on the input amplitude A. Since most of the RF circuits are compressive (i.e. $a_1 a_3 < 0$), the receiver gain falls as much as the input amplitude rises, determining a gain compression. This effect is defined by the 1-dB compression point (P_{1dB}): it represents the input signal level that causes a gain drop of 1 dB with respect to the ideal value. The P_{1dB} is the upper bound of the input signal power, because the compression introduces distortion on amplitude-modulated signal. Without an external filtering, as in the case of a SAW-less receiver, the gain

compression can occur even with large out-of-band blockers, causing receiver desensitization (i.e. SNR degradation).

1.2.2 Reciprocal and Harmonic Mixing

In a RF receiver, the mixers perform the downconversion of the input signal in baseband through a multiplication with a sinusoidal signal provided by a local oscillator (LO). Ideally this signal is a pure tone (i.e. an impulse in the frequency domain), but a realistic LO suffers from phase noise (random frequency variations of the signal) which gives rise to a broadened spectrum. The convolution between the noisy LO and an unfiltered blocker at the receiver input produces the downconversion in baseband of both the LO and blocker noise (Fig.

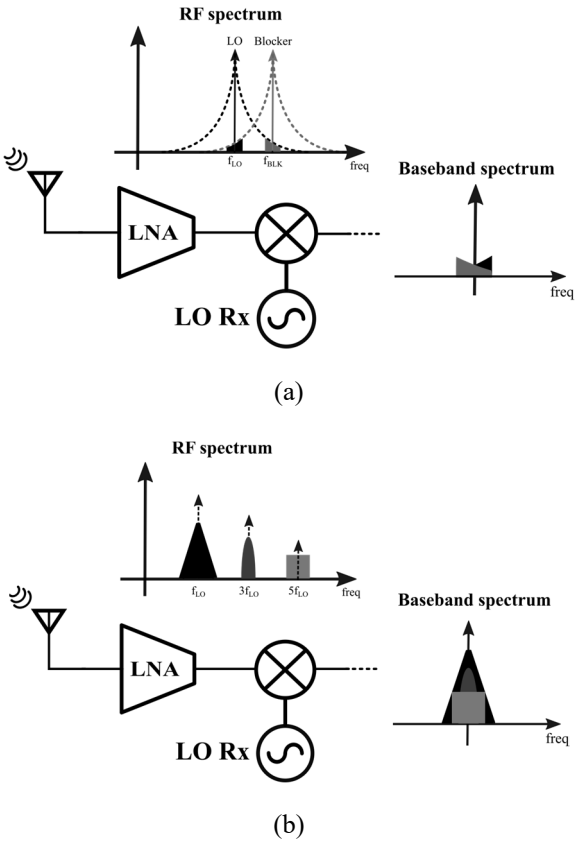

Figure 1.4: Reciprocal (a) and harmonic (b) mixing

1.4a), degrading the receiver NF: this effect is defined reciprocal mixing. Moreover, a realistic RF mixer multiplies the input signal by a square-wave, even though the oscillator generates a sinusoidal tone. Therefore, it is necessary to consider all the odd harmonics of the LO signal, which fold any signal located at these frequencies (Fig. 1.4b): this effect is the harmonic mixing.

1.2.3 Intermodulation

Assuming, at the input of the receiver, two strong interferences, at ω_1 and ω_2, which accompany the desired signal at ω_0, and the nonlinear behavior as described in (1.2): the output of the system will shows some further components generated by the mixing of these interferences. Without going into details, expanding the equation (1.2) with an input signal $x(t) = A_1 \cos(\omega_1 t) + A_2 \cos(\omega_2 t)$, the output exhibits the third-order intermodulation products at $2\omega_1 - \omega_2$ and $2\omega_2 - \omega_1$. If the frequency of the desired signal meets the condition $\omega_0 = 2\omega_1 - \omega_2$, one of these intermodulation products falls in the Rx band, corrupting the signal (Fig. 1.5). The power of the intermodulation products is a function of the interferences amplitude and the system linearity; in order to meet the standard requirements without an external filtering, the only way to limit the degradation of the receiver sensitivity is improving its linearity (challenging receiver design).

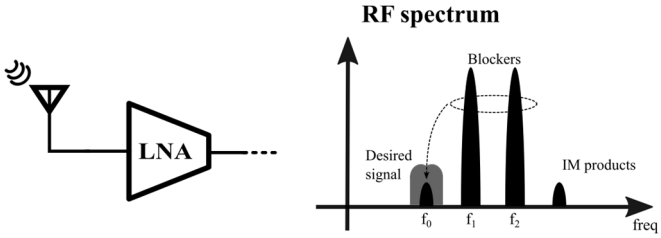

Figure 1.5: Intermodulation

1.2.4 Transmitter Noise Leakage

Finally, another issue that arises from the lack of an external filtering is the out-of-band noise generated by the transmitter. This noise falls in the Rx band, determining an higher equivalent NF and thus degrading the receiver sensitivity. This problem will be addressed in detail in Chapter 2.

1.3 SAW-less architecture

In this section will be given a conceptual overview of a SAW-less transceiver for FDD based standards. As introduced in Section 1.1, even though in an ordinary multi-standard transceiver several SAW filters are employed, it is possible to identify two main types of application. Usually the main transceiver, in which the transmitter and the receiver share the same antenna, needs a SAW-based duplexer (i.e. a double band-pass filter) to distinguish Tx and Rx channel: at the output of the transmitter it allows to filter out the harmful out-of-band components (harmonics and noise), in order to meet the standard specifications and avoid receiver desensitization; at the input of the receiver, it discriminates the weak Rx signal reducing the undesired blockers (local Tx signal included). A typical external duplexer reduces the power of the Tx signal by 50dB and the power of the received blocker signal by 55dB, drastically relaxing the receiver linearity requirements. Moreover, in a MIMO structure, other diversity receivers are used to improve the quality and the reliability of a Rx channel; at the input of these receivers, a SAW filter is used for the purposes already explained. In the designed SAW-less architecture, whose diagram block is shown in Fig. 1.6, the previously described challenges have been addressed and resolved to meet the standard specification; moreover, all the key blocks have been designed and physically realized to verify their performance. In the following sections a brief overview of the building blocks and their features is reported: the main receiver with the

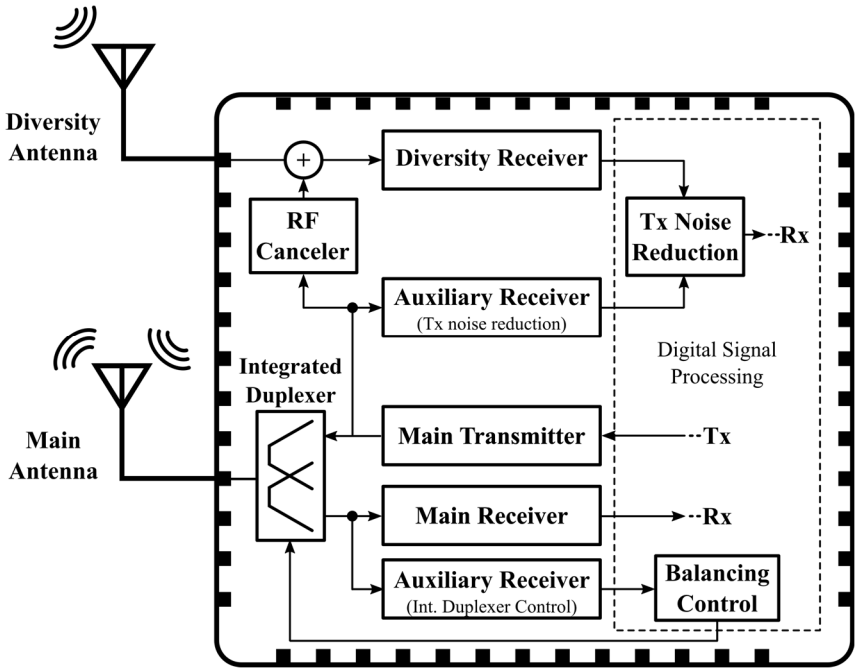

Figure 1.6: Conceptual overview of the proposed SAW-less platform

integrated duplexer is the solution proposed in [2], the diversity receiver with the RF canceler is the architecture [3] and the auxiliary receiver for the Tx noise monitoring is [4]. The digital blocks, that are the balancing control for the HT-based receiver and the Tx noise reduction in the diversity receiver, will be extensively deepen in the other chapters as they represent the main topics of this thesis.

1.3.1 Main Receiver with Integrated Duplexer

The Hybrid Transformer (HT) is a well-known circuit commonly used in telephone plant to cancel the echo-crosstalk. Recently, it has been proposed in several configurations to replace multiple off-chip duplexers, each operating on a single band, with a single reconfigurable and integrated system, thus reducing cost, complexity and area of FDD transceivers in handset devices. A HT-based duplexer allows the transmitter and the receiver to share the same antenna, ensuring a good

decoupling level between Tx and Rx path. Since the Tx is the most powerful signal among the out-of-band interferences, the HT helps to relax the linearity requirements of the receiver. However, the amplitude of the Tx signal that leaks in the receiver path is not fixed as in SAW-based duplexer, where the isolation is guaranteed through filtering, but it depends on the balancing condition of the hybrid transformer (this issue will be deepen in the Chapter 3). Moreover, even though the Tx signal is partially attenuated, external signals pass unfiltered through the HT, and the intermodulation products, generated by the mixing between external blocker and Tx leakage, could give rise to Rx desensitization. This problem has been addressed designing a low-power highly-linear receiver; only 45dB of Tx-Rx isolation are sufficient to meet the standard specifications.

1.3.2 Diversity Receiver with RF canceler

As represented in Fig. 1.2, at the input of a SAW-less receiver there are interferences coming from the external environment and from local transmitter. Considering the architecture schematized in Fig. 1.6, due to the near field coupling between the two antennas, part of the Tx signal leaks at the input of the diversity receiver. The finite linearity and the reciprocal mixing of the Tx leakage with the phase noise of the local oscillator could bring the diversity receiver to desensitization. To address these problems, a receiver with high linearity is proposed; however, in order to improve the linearity of the entire receiver chain, a RF self-interference canceler is introduced. This tunable circuit acts like a vector modulator: it provides at the input of the LNA a properly modulated copy of the signal sensed at the transmitter output, with the aim to reduce the Tx signal. The canceler is realized with two passive variable attenuators, a resistive and capacitive digital-to-analog-converter, and it ensures more than 25dB of Tx signal reduction when correctly programmed.

1.3.3 Auxiliary Receiver for Tx Noise Monitoring

Previous subsection has briefly introduced the solution that addresses the issues induced by the out-of-band Tx signal. However, even the transmitter broadband noise that directly falls into the Rx band can degrades the diversity receiver sensitivity. In order to face this problem, an auxiliary receiver is connected to the transmitter output to provide a baseband copy of the Tx noise that falls in the Rx band. This auxiliary receiver is characterized by low power demand and a high dynamic range: it is able to withstand the large transmitted signal without compressing (high 1-dB compression point), retaining a good sensitivity (low input-referred noise). In order to relax the requirements of the following blocks, the first stage of the auxiliary receiver consists of a band-reject N-path filter. These circuits have both high selectivity and linearity and, tuned to the Tx carrier, it ensures an attenuation of the large transmitted signal of about 20dB. Then, the downconversion chain is tuned to the Rx carrier frequency, providing a baseband copy of the Tx noise in the receive band. Finally, through a digital cancellation process, which will be introduced in the next section and deeply described in Chapter 2, the noise figure of the diversity receiver is restored.

1.3.4 Digital Signal Processing: HT Balancing Control and Tx Noise Reduction

The systems described so far represent the RF front-end of a SAW-less receiver; however, the overall architecture requires some digital assistance to work properly. Although the auxiliary receiver, shortly presented in the previous section, monitors the Tx noise in the Rx band, the effective noise reduction is carried out in the digital domain, where an equalizer allows to restore the sensitivity of the diversity receiver, degraded by the broadband Tx noise, without compromising the quality of the desired Rx signal. Moreover, the HT-based receiver presented in Section 1.3.1, requires at least 45dB of Tx-Rx isolation level to meet

the specifications, but one of the main issues of HT-based duplexers is the sensitivity of the isolation to the antenna impedance. In fact, the antenna impedance varies with time due to interactions with the external environment. Therefore, a low-power control network (auxiliary path + digital control system) is required to automatically and adaptively adjust the HT balancing to follow the antenna impedance time variations, keeping high the isolation level. The design of these digital blocks, the equalizer for the Tx noise reduction in the diversity receiver and the balancing control for the hybrid transformer-based receiver, will be extensively discussed in the following chapters.

Chapter 2

Digital Tx Noise Reduction in SAW-Less Diversity Receivers

In this Chapter, the complete architecture designed to restore the sensitivity of a SAW-less diversity receiver corrupted by the broadband transmitter noise is presented. Section 2.1 briefly introduces some of the solutions recently proposed in literature that address this topic. An overview of the system and considerations regarding signals levels are reported in Section 2.2. The digital equalization process, the noise cancellation issues, the baseband system requirements and the simulation results are analyzed in Section 2.3. Finally, the experimental results of the complete system are shown in Section 2.4.

2.1 Self-interference Reduction: State of the Art

As introduced in Chapter 1, in a common multi-standard platform many off-chip SAW filters are used to mitigate out-of-band interference; however, these filters are bulky, expensive, and have a fixed frequency response. SAW-less architectures can drastically simplify the system but several problems need to be addressed removing the RF filtering. Most of the proposed SAW-less solutions concentrate on blocking issues due to the main Tx signal rather than on broadband Tx noise which falls in the receiver band. To address this issue, in hybrid-transformer based duplexers a double notch has been demonstrated [6], in order to achieve high isolation between the transmitter and the receiver in both Tx and Rx band, reducing the strong Tx signal and the Tx noise in the received band. This solution, however, shows a challenging control of the hybrid transformer balance impedance, requiring a large number of tuning steps, and the integrated passive components occupies a large area (8.28 mm^2). Going toward more

digitally intensive transceiver architectures, the out of band emissions of the transmitter are mainly determined by the RF-DAC quantization noise. Even if 10 bits are sufficient to meet the 3G/4G in-band and ACLR performance requirements, the Rx-band noise requirements are more stringent. An all-digital transmitter with configurable spectral shaping of the out-of-band noise in the Rx-band has been recently proposed [7]. Through a ΔΣ modulator and mismatch shaping techniques, the authors are able to reduce the Tx noise in the Rx band down to -160 dBc/Hz. However, for high transmitted power levels, this could not be sufficient.

2.2 Receiver Sensitivity Degradation

Assuming a MIMO structure and FDD standards, the coupling between the main and the diversity antenna produces, at the input of the secondary receiver, strong self-interferences coming from the local transmitter. The Tx spectrum can be considered as composed by a strong modulated signal and a broadband noise: if the main signal can be treated like the strongest out-of-band blocker, which worsen the diversity Rx performance due to the nonlinear effects (compression, intermodulation, etc.), the portion of Tx noise which falls in the Rx band raises the effective noise figure of the receiver thus degrading its

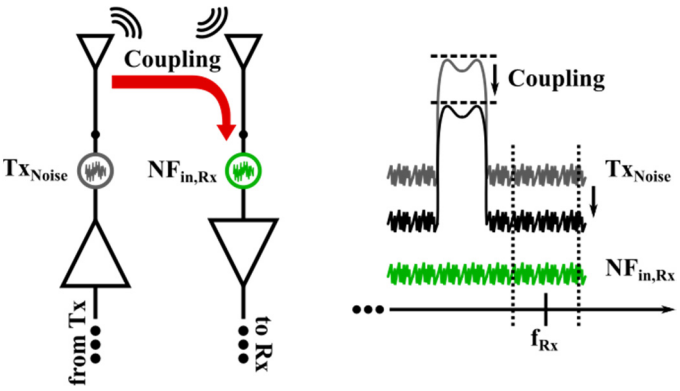

Figure 2.1: Sensitivity degradation

sensitivity (Fig. 2.1). Considering the power spectral density [dBm/Hz] of the Tx noise defined as

$$N_{Tx} = P_{Txn} + P_{Tx} \tag{2.1}$$

where P_{Tx} [dBm] is the transmitter power and P_{Txn} [dBc/Hz] is the noise power related to the Tx carrier signal, the noise at the input of the diversity receiver is equal to

$$P_{Txn,Rx} = N_{Tx} - CP \tag{2.2}$$

in which CP [dB] is the coupling factor between the two antennas. For example, assuming P_{Tx} = 23dBm (full power of the transmitter), P_{Txn} = -155dBc/Hz and CP = 25dB, the maximum Tx noise power at the input of the receiver will be $P_{Txn,Rx}$ = -157dBm/Hz. Assuming the diversity receiver characterized by its noise figure NF_{Rx} [dB], the Tx noise gives rise to an effective noise figure $NF_{Eff,Rx}$ [dB] which can be estimated as follows

$$NF_{Rx,Eff} = 174 + 10\log\left(10^{\frac{-174+NF_{Rx}}{10}} + 10^{\frac{P_{Txn,Rx}}{10}}\right) \tag{2.3}$$

or, equivalently, which corresponds to a noise figure degradation ΔNF_{Txn} [dB] equal to

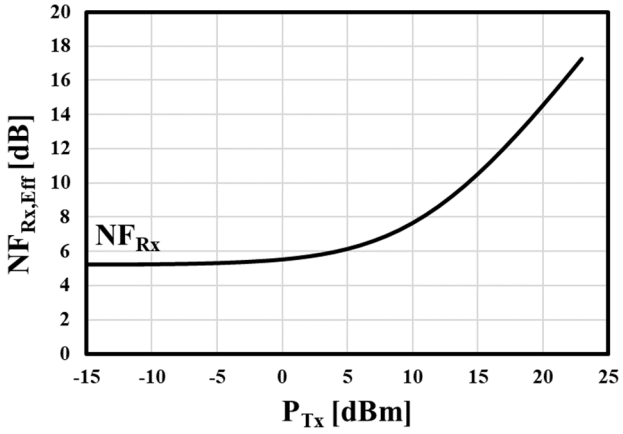

Figure 2.2: Diversity receiver NF degradation versus Tx power

$$\Delta NF_{Txn} = 10\log_{10}\left(10^{\frac{P_{Txn,Rx}+174-NF_{Rx}}{10}}+1\right) \quad (2.4)$$

The result is shown in Fig. 2.2: the higher is the transmitter power P_{Tx}, and hence the Tx noise at Rx input $P_{Txn,Rx}$, the higher is the sensitivity degradation of the diversity receiver. Considering that, in this project, the receiver is [3], its noise figure is approximatively NF_{Rx} = 5.2 dB; in the worst case (transmitter at full power) the effective noise figure of the diversity receiver is $NF_{Rx,Eff} \approx$ 17 dB, which corresponds to a degradation $\Delta NF_{Txn} \approx$ 12 dB with respect to the NF_{Rx}.

2.2.1 Overview Proposed Architecture

Figure 2.3 shows a simplified block diagram of the architecture proposed to recover the sensitivity of a SAW-less diversity receiver [3]. In a realistic application, at the input of the receiver there is the desired signal corrupted by the transmitted noise which falls in the Rx band. Since there is no distinction in frequency domain between noise and desired signal, the standard filters with frequency specifications domain are useless. However, a digital filter based on an adaptive equalizer could reduce this noise and restore the receiver sensitivity without degrading the desired Rx signal. In order to work properly, the digital equalizer should know the signal to be filter out, or at least one

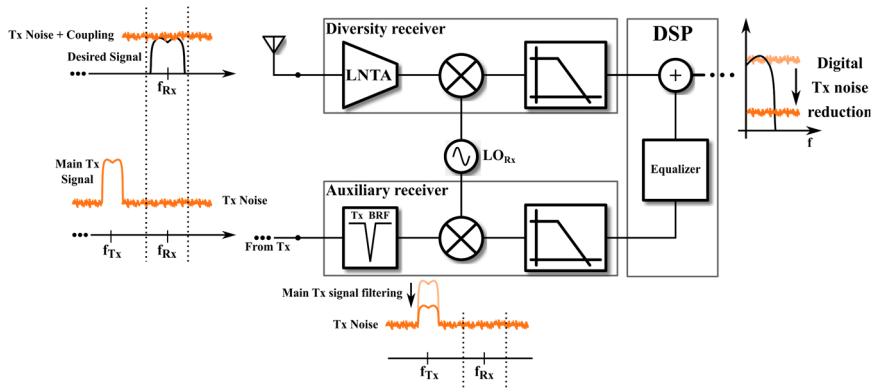

Figure 2.3: Conceptual overview of the proposed architecture

correlated with it. The external Rx signal is completely unknown and uncorrelated with the Tx noise which comes from the local transmitter. An auxiliary receiver [4], whose first stage consists of a band-reject filter tuned to the Tx carrier to attenuate the main signal, senses the Tx noise in Rx band at the output of the transmitter, providing this signal to the digital system. It is clear that this is in some way correlated with the noise which degrades the diversity receiver: the digital equalizer is able to filter out the noise at the output of the diversity receiver, without affecting the desired signal, properly matching the transfer function between the two antennas, restoring the receiver specifications.

2.2.2 Signal Levels Considerations and Required Digital Noise Reduction

The performance of the proposed architecture depend on the auxiliary receiver and the digital equalizer specifications. It is possible to estimate the final result carefully analyzing the signal levels in the whole system; for this purpose, the architecture shown in Fig. 2.3 is now represented in Fig. 2.4 differently to focus on the system

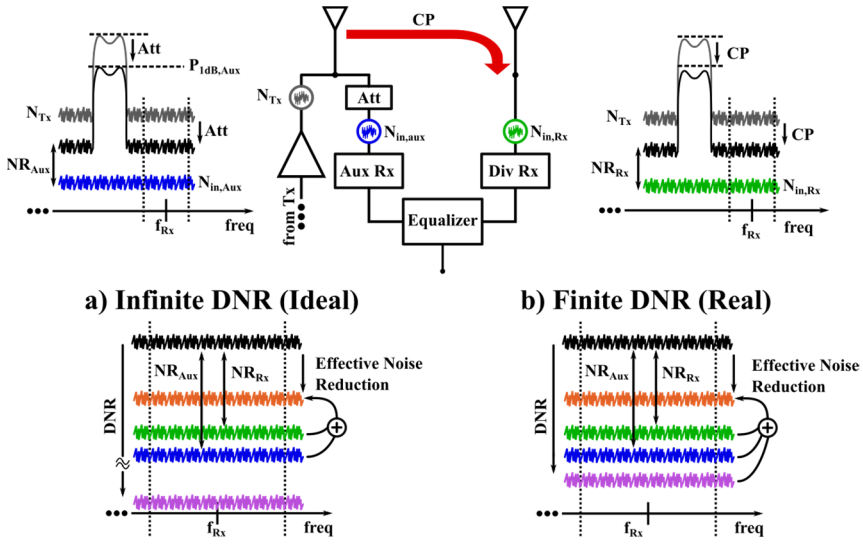

Figure 2.4: Signal levels considerations and effective noise reduction with a) Infinite DNR and b) Finite DNR

specifications. In order to simplify the argument, it is assumed that there is no external signal but only the self-interferences (being uncorrelated with the Tx noise, the results would be the same but more difficult to be evaluated); moreover, at first an ideal digital circuit able to ensure an infinite digital noise reduction (DNR) is assumed (Fig. 2.4a), where only the auxiliary receiver noise might contribute to degrade the diversity receiver noise figure. The auxiliary receiver [4] is characterized by its 1-dB compression point $P_{1dB,Aux}$ [dBm], noise figure NF_{Aux} [dB] and gain G_{Aux} [dB], whereas the diversity receiver [3] is characterized by its noise figure NF_{Rx} [dB] and gain G_{Rx} [dB]. In front of the auxiliary, the variable attenuator adapts the attenuation level Att [dB] depending on the transmitter power, in order to keep the maximum signal power at the compression level and thus fixing the Tx noise level at the input of the auxiliary; the attenuation function is defined as

$$Att = P_{Tx} - P_{1dB,Aux} \tag{2.5}$$

and Tx noise at the input of the auxiliary receiver is

$$P_{Txn,Aux} = N_{Tx} - Att \tag{2.6}$$

Regarding the diversity, the coupling factor between the main and the secondary antenna CP [dB] is assumed fixed, therefore the Tx noise level at the input of the diversity changes with the transmitter power P_{Tx}, as expressed in (2.2). Considering that, in the proposed architecture the bandwidth of interest is 20MHz at RF, the frequency response of the coupling between the two antennas is almost flat in this bandwidth [8] and hence CP can be approximated constant. Similarly to the SNR, it is possible to define a noise ratio (because in this case also the signal is a noise) for the auxiliary NR_{Aux} [dB] and the diversity path NR_{Rx} [dB] respectively as ratio between the Tx noise at the input of the receivers ($P_{Txn,Aux}$ and $P_{Txn,Rx}$) and the characteristic noise of the chains referred to their input ($N_{in,Aux}$ and $N_{in,Rx}$):

$$NR_{Aux} = P_{Txn,Aux} - N_{in,Aux} = P_{Txn,Aux} - \left(-174 + NF_{Aux}\right) \tag{2.7}$$

$$NR_{Rx} = P_{Txn,Rx} - N_{in,Rx} = P_{Txn,Rx} - \left(-174 + NF_{Rx}\right) \tag{2.8}$$

In the digital domain, since the equalizer has to match the Tx noise levels at the output of the diversity and the auxiliary receiver in order to maximize the noise cancelling, the equalizer gain G_{eq} [dB] compensates the different gains of the two paths, and it will be

$$G_{eq} = (G_{Rx} - Cp) - (G_{Aux} - Att) \tag{2.9}$$

As previously said, only the auxiliary noise might degrade the effective noise figure after the digital equalization if an infinite DNR is assumed. If the Tx noise levels of the two paths are equalized, the difference ΔN_{Aux} [dB] between the auxiliary and the diversity noise is determined by the two noise ratios

$$\Delta N_{Aux} = NR_{Rx} - NR_{Aux} = NF_{Aux} + Att - (CP + NF_{Rx}) \tag{2.10}$$

and the noise figure degradation ΔNF_{Aux} [dB] of the diversity receiver is given by the following expression

$$\Delta NF_{Aux} = 10\log_{10}\left(10^{\frac{\Delta N_{Aux}}{10}} + 1\right) \tag{2.11}$$

Figure 2.5 shows the relation between the NF_{Rx} degradation and the Tx power, hence the Tx noise level which couples at the diversity input. Assuming the system specifications as reported in Tab. 2.1, the transmitter at full power the attenuation level Att = 18dB from (2.5) and

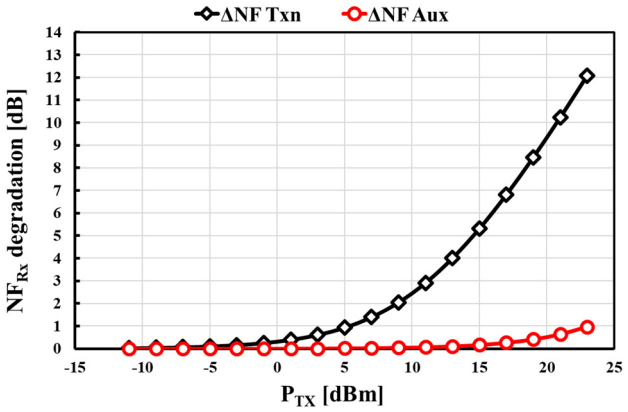

Figure 2.5: Diversity receiver NF degradation versus Tx power, with (circles, infinite DNR) and without (squares) Tx noise reduction

ΔN_{Aux} = -6dB from (2.10), determining a ΔNF_{Aux} = 0.97dB in the worst case. Without the Tx noise reduction the degradation would have been ΔNF_{Txn} = 12.08dB (2.4), affecting the diversity receiver sensitivity. It is worth to note that, decreasing the Tx power P_{Tx}, the degradation shrinks down because the attenuation before the auxiliary receiver can be reduced, thus keeping unchanged the noise ratio NR_{Aux}, but the NR_{Rx} decreases, determining a lower ΔN_{Aux} and hence a lower ΔNF_{Aux}.

Although an infinite DNR has been assumed (Fig. 2.4a) so far, and the noise figure degradation (Fig. 2.5 circles) was only due to the limited dynamic range of the auxiliary receiver, it is necessary to consider that the digital equalizer has finite performance as well: for example, quantization noise and approximation level of the equalized signal can limit the noise reduction. Therefore, the residual Tx noise after the cancellation can compromise the diversity receiver sensitivity, increasing its effective noise figure. As done before for the auxiliary receiver noise, the NF degradation due to the finite DNR can be estimated by computing the difference between the diversity receiver noise and the residual Tx noise after the digital cancellation, referring the noise levels at the input of the diversity. Assuming *DNR* [dB] the Tx noise reduction achieved with the digital cancellation, the difference ΔN_{DNR} [dB] between the residual Tx noise and the diversity noise is

TABLE 2.1
SUMMARY RF PATH SPECIFICATIONS

P_{Tx}	23 dBm (full power)
P_{Txn}	-155 dBc/Hz
NF_{Rx}	5.2 dB
CP	25 dB
NF_{Aux}	6.2 dB
$P_{1dB,Aux}$	5 dBm
G_{Rx}	35 dB
G_{Aux}	30 dB

$$\begin{aligned}\Delta N_{DNR} &= \left(P_{Txn,Rx} - DNR\right) - N_{in,Rx} = \\ &= \left(P_{Txn} + P_{Tx} - CP - DNR\right) - \left(-174 + NF_{Rx}\right)\end{aligned} \tag{2.12}$$

which results in a noise figure degradation ΔNF_{DNR} [dB] equal to

$$\Delta NF_{DNR} = 10\log_{10}\left(10^{\frac{\Delta N_{DNR}}{10}} + 1\right) \tag{2.13}$$

Although the ΔNF_{Aux} mainly depends on the dynamic range of the auxiliary receiver [4] employed in the proposed system, and hence it is assumed as a given value, the ΔNF_{DNR} depends on the digital equalizer performance, whose design is presented in this work. Therefore, it is possible to define a minimum desired DNR level (that will be a system specification) which allows not to further compromise the effective noise figure of the diversity receiver after the cancellation. In order to evaluate the NF increase due to the finite DNR with respect to the degradation only due to the auxiliary noise, the additional NF degradation $\Delta NF_{DNR,Add}$ [dB] is defined as follows

$$\Delta NF_{DNR,Add} = 10\log_{10}\left(\frac{10^{\frac{\Delta N_{DNR}}{10}}}{10^{\frac{\Delta N_{Aux}}{10}} + 1} + 1\right) \tag{2.14}$$

The result is shown in Fig. 2.6: the higher is the DNR, the lower is the NF degradation added to ΔNF_{Aux} by the limited performance of the digital path; assuming $\Delta NF_{DNR,Add} \leq 0.1$dB as acceptable further degradation in the worst case (transmitter at full power), the required DNR should be greater than 28dB. Finally, the total NF degradation ΔNF_{Tot} [dB] of the diversity receiver noise figure, given by the sum of the auxiliary receiver noise and residual Tx noise after the DNR, is expressed as

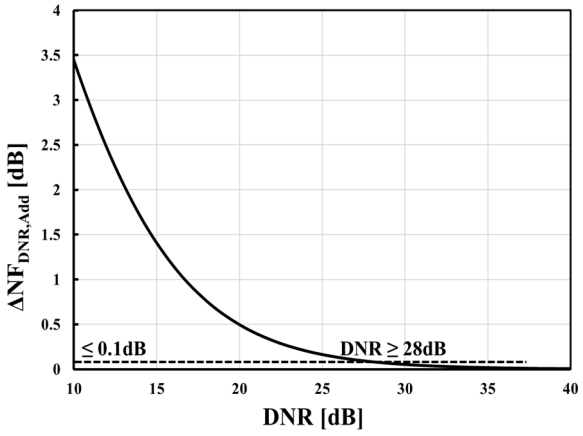

Figure 2.6: Additional NF degradation versus DNR

$$\Delta NF_{Tot} = 10\log_{10}\left(10^{\frac{\Delta N_{Aux}}{10}} + 10^{\frac{\Delta N_{DNR}}{10}} + 1\right) \qquad (2.15)$$

Figure 2.7 reports the overall degradation of the diversity receiver NF changing the transmitted power, assuming real performance of both auxiliary receiver and the digital equalizer. Here a *DNR* of 28dB is assumed, demonstrating that the NF worsening related to a finite DNR can be negligible if a sufficient cancellation level is ensured. In the worst case, the total NF degradation is ΔNF_{Tot} = 1.05dB, resulting in an

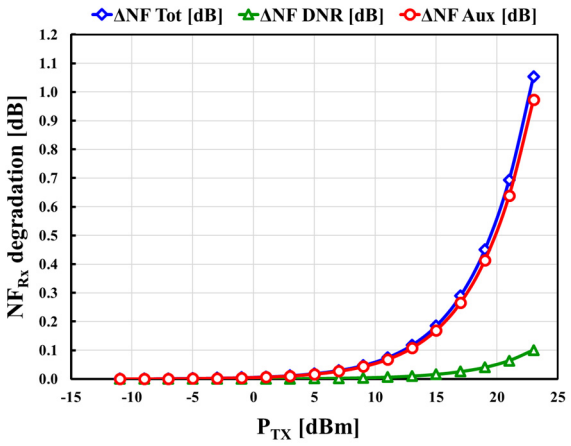

Figure 2.7: Total NF degradation and its contributors versus Tx power, assuming 28dB of DNR

improvement of about 11dB with respect to the NF degradation without noise reduction, that is ΔNF_{Txn} = 12.08dB. The design of the digital path will be discussed in the next sections.

2.3 Digital Equalization

The analysis carried out in Section 2.2.1 has demonstrated that, with the given configuration (Tab. 2.1) of the proposed architecture (Fig. 2.3), more than 28dB of Tx noise reduction are needed in order to consider negligible the residual Tx noise after the cancellation. The signal processing is performed in the digital domain, where the baseband signal provided by the auxiliary receiver is properly processed by the equalizer and then subtracted from the diversity receiver's signal. The purpose of the digital equalizer is to match the difference between the diversity and the auxiliary path; a simplified block diagram of the system is represented in Fig. 2.8.

2.3.1 System model

Regarding the digital path, the signal of interest is only the Tx noise which falls in the Rx band and hence the transmitter can be simply modeled as a white noise generator. Since the specification of the digital canceler has been already defined, the auxiliary and the diversity

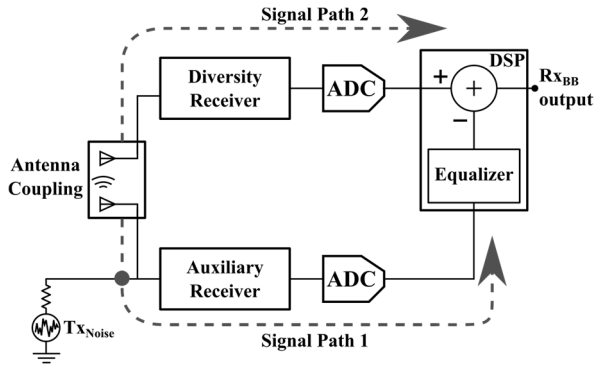

Figure 2.8: Simplified system model

receiver are assumed as ideal paths, which downconverts a signal bandwidth of 20 MHz around the Rx carrier frequency, without introducing impairments. Moreover, at first approximation, the analog-to-digital converters (ADC) are considered ideal as well (negligible quantization noise). Therefore, considering that the auxiliary receiver senses the signal at the output of the transmitter, whereas the diversity receives the self-interference from the antenna, the digital path should equalize, in baseband, the RF coupling between the main and the diversity antenna. In [8] the coupling between two Planar Inverted-F Antennas (PIFA), widely used in mobile communication systems for their low costs and small size, has been analyzed in real working conditions and measured in different positions to simulate the displacement that they have in a modern smartphone. In all cases, the magnitude of the coupling is almost flat in the band of interest, ensuring less than 1dB of variation over 20 MHz, whereas the phase variation over the same bandwidth gives rise to a group delay of about 3-4 ns. Therefore, the task the digital equalizer has to perform would seem quite simple, mainly characterized by gain and delay control of the signal. However, the interaction of the antennas with the external environment changes the coupling features over time, hence an adaptive equalizer is needed; furthermore, unlike the common implementations, in this application the digital path has to process a broadband noise, which cannot be modelled as a band-limited signal, making the equalization process quite tricky, as will be explained later.

2.3.2 Optimum Wiener Filter and Adaptive Least Mean Square Algorithm

In literature there is a huge number of studies formulated to model a wireless channel and methods developed to equalize its behavior. However, in the system under consideration, the simplicity of the coupling model between the two local antennas, the rather low level of desired cancellation and the aim of a low-cost digital path suitable for a mobile application suggest designing an equalizer based on an

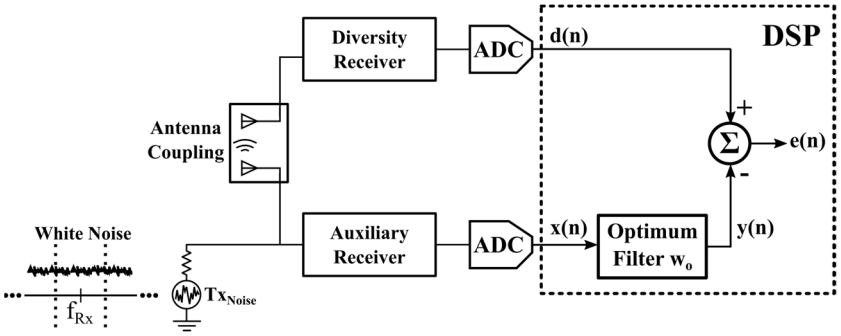

Figure 2.9: Ideal implementation of digital equalizer: optimum Wiener filter

adaptive Least Mean Square (LMS) finite impulse response (FIR) filter. The well-known LMS algorithm [9] is a recursive method belonging to the Wiener filtering theory [10]; it is widely used in adaptive linear filtering, ensuring a good compromise among computational requirements, rate of convergence, steady-state error and robustness. The Wiener filter represents the optimal solution to which this method converges iteratively and, although it is not used in realistic applications, the study of the Wiener solution allows to understand performance and limits of a LMS FIR filter. In order to generalize the discussion in the following sections, all the theory will be formulated in complex form and the signals are assumed wide-sense stationary and zero-mean. Initially, an equalizer based on a *N*-order linear filter, whose coefficients w_o give rise to the optimum Wiener filter (Fig. 2.9), is considered. Given the input signal *x(n)*, the filter output *y(n)* is

$$y(n) = \sum_{i=0}^{N-1} w_{oi}^{*} x(n-i) \tag{2.16}$$

where the asterisk denotes complex conjugations. It is the estimate of the desired signal *d(n)* which minimizes a cost function ξ represented by the mean square value (MSE) of the estimation error *e(n)*

$$\xi = E\left[e(n)e(n)^{*} \right] = E\left[\left| e(n) \right|^{2} \right] \tag{2.17}$$

where *E* indicates the statistical expectation operator, and the error *e(n)* is the difference between *y(n)* and *d(n)*

$$e(n) = d(n) - y(n) \tag{2.18}$$

In the proposed architecture, the unknown signal *d(n)* is the output of the diversity receiver, and the equalizer input *x(n)* is the auxiliary receiver signal, which is correlated with *d(n)*. The optimum filter minimizes the mean square value of the estimation error (2.17), allowing to subtract an equalized signal from the diversity receiver output thus reducing the undesired Tx noise; the residual noise relies on the equalizer performance. According to the Wiener theory, the optimal coefficients w_o depend on the autocorrelation function of the filter input *x(n)* and the cross-correlation between the filter input and the desired response *d(n)*. In general, the correlation between two signals represents a statistical relationship which involves a certain dependence. For a given time shift *k,* the cross-correlation between *x(n)* and *d(n)* can be defined as

$$p(-k) = \sum_{n=-\infty}^{+\infty} x(n-k)d^*(n) = E\left[x(n-k)d^*(n)\right] \quad k = 0, \pm 1, \ldots \tag{2.19}$$

whereas the autocorrelation, which involves only a signal (e.g. *x(n)*), is expressed as

$$r(k) = \sum_{n=-\infty}^{+\infty} x(n)x^*(n-k) = E\left[x(n)x^*(n-k)\right] \quad k = 0, \pm 1, \ldots \tag{2.20}$$

The autocorrelation sequence of a signal reaches its maximum value for k=0, because the signal matches perfectly with itself at zero time shift. Focusing on the addressed case, the *Wiener-Hopf* equations [10] need to be solved in order to find the optimum N-order FIR filter. Exploiting matrix notation, the filter input sequence is represented as

$$\mathbf{x}(n) = \left[x(n), x(n-1), \ldots, x(n-N+1)\right]^T \tag{2.21}$$

where N is the filter order and ^{T} indicates transposition, whereas the coefficients vector of the optimum filter are

$$\mathbf{w}_o = \left[w_{o1}, w_{o2}, \ldots, w_{oN-1}\right]^T \tag{2.22}$$

Introducing the N-by-N autocorrelation matrix **R** of the input signal

$$\mathbf{R} = E\left[\mathbf{x}(n)\mathbf{x}^H(n)\right] = \begin{bmatrix} r(0) & r(1) & \cdots & r(N-1) \\ r^*(1) & r(0) & \cdots & r(N-2) \\ \vdots & \vdots & \ddots & \vdots \\ r^*(N-1) & r^*(N-2) & \cdots & r(0) \end{bmatrix} \tag{2.23}$$

in which ^{H} denotes Hermitian transposition and the *r(k)* element is defined as (2.20), and the cross-correlation vector **p** between the input of the filter and the desired signal

$$\mathbf{p} = E\left[\mathbf{x}(n)d^*(n)\right] = \left[p(0), p(-1), ..., p(1-N)\right]^T \tag{2.24}$$

where the *p(-k)* element is computed as (2.19), the Wiener-Hopf equations can be is expressed as

$$\mathbf{w}_o = \mathbf{R}^{-1}\mathbf{p} \tag{2.25}$$

where $^{-1}$ indicates matrix inversion. Therefore, in order to find the best coefficients of the digital equalizer based on a Wiener filter, it is necessary to know the autocorrelation matrix of the filter input and the cross-correlation vector between the input and the desired response. Moreover, it is possible to determine the minimum MSE produced by the optimum Wiener filter, which represents the residual Tx noise after the cancellation in the described application. Assuming the optimal coefficients $\mathbf{w}_o$ computed in (2.25), the error *e(n)* (2.18) is equal to

$$e(n) = d(n) - y(n) = d(n) - \mathbf{w}_o^H \mathbf{x}(n) \tag{2.26}$$

and the minimum MSE (2.17) is expressed as follows

$$\begin{aligned} \xi_{\min} &= E\left[e(n)e(n)^*\right] = E\left[\left|d(n)\right|^2\right] - E\left[\left|y(n)\right|^2\right] = \\ &= \sigma_d^2 - \mathbf{p}^H \mathbf{w}_o = \sigma_d^2 - \mathbf{p}^H \mathbf{R}^{-1}\mathbf{p} \end{aligned} \tag{2.27}$$

where σ_d^2 indicates the variance (i.e. the power) of the desired signal. A digital equalizer based on a Wiener filter is not actually implemented, because it requires a priori information about the statistics of the input signals, which may not be available or may change in a non-stationary

environment, and the coefficients estimation (2.25) requires a matrix inversion, which involves a high computational complexity, nevertheless it represents the optimum solution to which the LMS algorithm converges recursively. Starting from an initial value for the filter coefficients **w** (usually **w**(0)=0), the algorithm converges to the optimum Wiener filter $\mathbf{w}_o$ iteratively adjusting the coefficients in order to minimize the MSE. The LMS algorithm is a s*tochastic gradient algorithm* because does not require the deterministic gradient in the recursive computation of the Wiener filter; it does not need any prior measurements about the statistics of the input signals or matrix inversion. Furthermore, it suits non-stationary environments, like the addressed case, being able to follow the time-variation of the equalized system, assuming these variations slower than the convergence time of the algorithm. An adaptive equalizer based on LMS algorithm (Fig. 2.10) is characterized by two basic processes: filtering and coefficients adaptation, defined in matrix form as follows

$$\begin{aligned} y(n) &= \mathbf{w}^H(n)\mathbf{x}(n) && \text{Filtering} \\ \mathbf{w}(n+1) &= \mathbf{w}(n) + \mu e^*(n)\mathbf{x}(n) && \text{Coefficients adaptation} \end{aligned} \tag{2.28}$$

where *e(n)* is the instantaneous error as in (2.18). The parameter μ is the step-size which has to be carefully chosen because it governs the behavior of the algorithm:

- Rate of convergence, and hence tracking capability;
- Stability;
- Misadjustment, which quantifies the difference between the final MSE obtained with the LMS algorithm and the minimum MSE produced by the optimum Wiener filter.

Although the step-size can be set to define the right balancing between rate of convergence and steady-state error, the performance of a Wiener filter, defined in (2.27), fix an upper bound of the results that an adaptive LMS FIR filter can reach realistically. Therefore, the expression (2.27) highlights that the power of the residual signal after the equalization only depends on the statistical parameters of the input signals.

2.3.3 Noise Cancellation Issues

As previously reported, with a digital equalizer based on an optimum Wiener filtering (Fig. 2.9), the resulting performance (2.27) only depend on the autocorrelation function of the reference signal *x(n)*, provided by the auxiliary receiver, and the cross-correlation between *x(n)* and the desired signal *d(n)* from the diversity receiver. In the addressed architecture, the signal of interest is the Tx noise which falls in the Rx band, and the easiest way to describe this signal is adopting a white noise model, a random signal with flat power spectral density (PSD) and statistical time independence. Considering that the PSD is related to the autocorrelation function via the Fourier transform

$$S(f) = \int_{-\infty}^{+\infty} r(\tau) e^{-j2\pi f\tau} d\tau \tag{2.29}$$

and assuming the reference signal *x(t)* modeled in continuous time (essentially before the analog to digital conversion) as white noise with constant PSD = N_0, the *x(t)* autocorrelation will be a Dirac Delta function

$$S_x(f) = N_0 \;\Rightarrow\; r_x(\tau) = E\left[x(t)x^*(t-\tau)\right] = N_0\delta(\tau) \tag{2.30}$$

Moreover, in order to simplify the following analyses, the coupling function between the main and the diversity antenna (Fig. 2.9) is assumed only characterized by its group delay, giving rise to a baseband signal delay. In this simplified model, the desired signal *d(t)* is a temporal shift of the reference one

$$d(t) = x(t-\gamma) \tag{2.31}$$

where γ denotes the delay introduced by the antenna coupling (i.e. the group delay). It is worth to recall that, in this analysis, diversity and auxiliary are considered ideal path. With these assumptions, the cross-correlation between reference and desired signal is

$$p_x(-\tau) = E\left[x(t-\tau)d^*(t)\right] = E\left[x(t-\tau)x^*(t-\gamma)\right] = N_0\delta(\tau-\gamma) \tag{2.32}$$

In continuous time, the cross-correlation corresponds to the impulsive autocorrelation of *x(t)* shifted by γ. Going into discrete time domain, the sampling period t_s sets the temporal resolution of signals and related statistical parameters: the autocorrelation of *x(n)* does not change, since the time independence of the samples still gives rise to an impulsive autocorrelation. However, considering that in discrete time $\tau = mt_s$, where *m* is an integer number, the cross-correlation between *x(n)* and *d(n)* will be

$$p(-mt_s) = E\left[x(n-mt_s)x^*(n-\gamma) \right] = N_0\delta(mt_s - \gamma) \qquad (2.33)$$

Therefore, in the digital domain, the cross-correlation between the reference and the desired signal is non-zero only if the antenna coupling group delay is perfectly multiple of the sampling period $\gamma = mt_s$. Obviously, this assumption is physically unrealistic and hence, from (2.27), it would seem impossible to reduce in digital domain the Tx noise due to its time independence. The white noise model used in the above considerations is unrealistic as well, but it allows to introduce what may limit the performance of the digital system. The equalizer does not have to process a band-limited signal, but a downconverted RF noise consisting of spurious emissions of the transmitter. Even though the signal of interest is a broadband noise, only a reduction of the noise in the Rx band is needed to restore the sensitivity of the diversity receiver, hence in a limited band. Since the power spectral density and the autocorrelation function of a signal are related via Fourier transform (2.29), a band-limited noise has a constant PSD only in a certain bandwidth and the related autocorrelation is non-zero in a certain timeframe. Both analog and digital filters give rise to a band-limited white noise, thus extending its autocorrelation, but only in the continuous time domain the cross-correlation (2.32), which represents the similarity between reference and desired signal, is surely not zero. A conceptual overview of the proposed system is reported in Fig. 2.10; it is worth to note that anti-aliasing low-pass filters are commonly used before ADCs, hence this solution does not complicate the whole architecture. Approximating the antenna coupling effects with a signal

delay, and assuming similar filtering on *x(t)* and *d(t),* the autocorrelation of the filtered signals $x_f(t)$ and $d_f(t)$ will depend on the filter specifications (explained in the following sections), and the resulting cross-correlation in continuous time will still correspond to the time-shifted autocorrelation of $x_f(t)$ and above all the corresponding discrete time cross-correlation will be not zero for some samples, making the digital equalization possible regardless the delay introduced by the antenna coupling. The following section will show that a suitable designed analog filtering before ADC allows the digital equalizer to work properly.

2.3.4 Analog Filtering and Signals Correlation

In previous sections, a digital equalizer based on a Wiener filtering approach has been proposed as solution to restore the sensitivity of a SAW-less diversity receiver corrupted by the Tx noise in Rx band. However, the statistical independence of the noise may limit the desired digital noise reduction (minimum DNR ≥ 28 dB). A solution, based on an analog low-pass filtering of the noise before the analog-to-digital conversion, has been supposed to extend the cross-correlation in discrete time domain between the reference signal provided by the auxiliary receiver and the desired response generated by the diversity. Assuming the analog filter as a linear time-invariant system, characterized by its impulse response *h(t)* and frequency response *H(f),* clearly the in-out relation is obtained through convolution between input and impulse response, but it is necessary to determine how the filter response shapes the autocorrelation of the output signal. In frequency domain, it can be demonstrated [11] that the PSD of the output is the product of the input PSD multiplied by the magnitude squared of the filter frequency response: for the reference signal results

$$S_{x_f}(f) = S_x(f)\left|H(f)\right|^2 \tag{2.34}$$

and equivalently for the desired signal if similar filtering is assumed. The autocorrelation of the output can be obtained applying the inverse Fourier transform to (2.34)

$$r_{x_f}(\tau) = \int_{-\infty}^{+\infty} S_x(f)\left|H(f)\right|^2 e^{j2\pi f\tau} df \tag{2.35}$$

If the input signal *x(t)* is a white noise with constant PSD $S_x(f)$=N_0, the PSD of the filtered signal will be

$$S_{x_f}(f) = N_0\left|H(f)\right|^2 \tag{2.36}$$

that is simply the squared-magnitude frequency response of the analog filter scaled by the PSD of the input, and the resulting autocorrelation is

$$r_{x_f}(\tau) = N_0 r_h(\tau) \tag{2.37}$$

where r_h indicates the autocorrelation of the analog filter impulse response. Considering an ideal LPF with cut-off frequency f_c, the

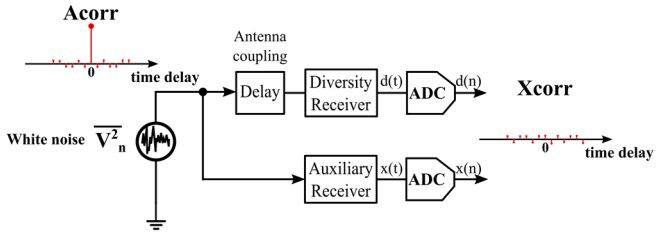

(a)

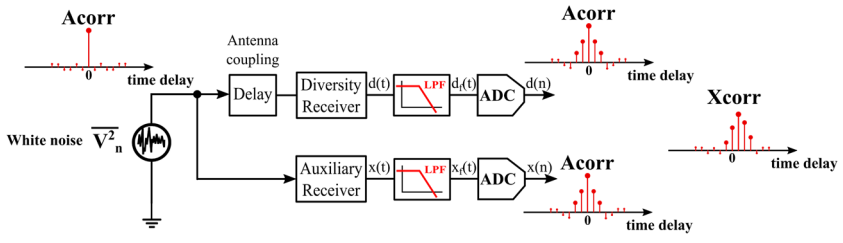

(b)

Figure 2.10: Conceptual overview of cross-correlation between reference and desired signal without (a) and with (b) analog filtering

filtered signal will be a windowed white noise (Fig. 2.11) with PSD expressed as

$$S_{x_f}(f) = N_0 rect(\frac{f}{2f_c}) = \begin{cases} N_0 & f \in [-f_c, f_c] \\ 0 & \text{elsewhere} \end{cases} \tag{2.38}$$

which gives rise to an autocorrelation function equal to

$$r_{x_f}(\tau) = N_0 2 f_c sinc\left(2\pi f_c \tau\right) \tag{2.39}$$

Assuming the same ideal LPF applied on the desired signal *d(t)*, and still approximating the coupling effects as a baseband signal delay γ, the resulting cross-correlation between the filtered signals $x_f(t)$ and $d_f(t)$ will be the autocorrelation introduced by the analog filters shifted by the group delay of the antenna coupling

$$\begin{aligned} p_{x_f,d_f}(-\tau) &= E\left[x_f(t-\tau)d_f^*(t)\right] = E\left[x_f(t-\tau)x_f^*(t-\gamma)\right] = \\ &= N_0 2 f_c sinc\left(2\pi f_c\left(\tau-\gamma\right)\right) \end{aligned} \tag{2.40}$$

The reported example is achieved with an ideal LPF, it highlights that limiting the noise bandwidth, through a proper analog filtering, determines a cross-correlation with (ideally) infinite length; in discrete-time domain it gives rise to a sampled sinc function shifted by γ, which is defined as

$$p_{x_f,d_f}(-mt_s) = N_0 2 f_c sinc\left(2\pi f_c\left(mt_s-\gamma\right)\right) \tag{2.41}$$

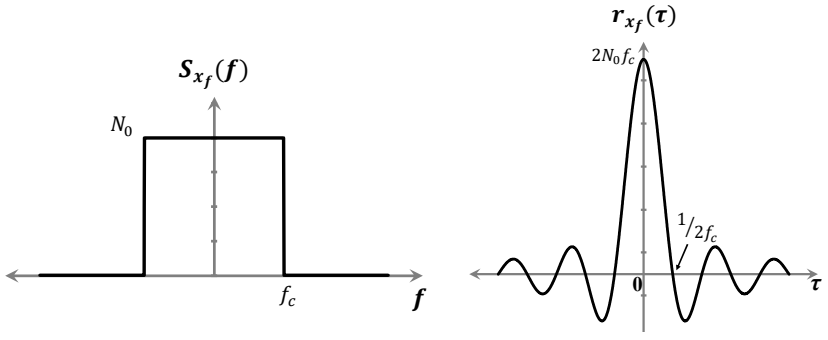

Figure 2.11: PSD and autocorrelation function of a band-limited white noise

The delay can still determine a weak correlation if the samples of the main lobe are missing, but it depends on several factors, for example sampling frequency, which can be chosen as needed (explained later). The most interesting result is the non-zero cross-correlation regardless the antenna coupling effects, which will allow the digital LMS filter to always find a certain dependency between reference and desired signal. Obviously, a LPF with a perfectly rectangular frequency response is an ideal approximation, but it allowed to clearly explain the result. In a realistic application it is necessary to define the specifications of these analog filters (design method, cut-off frequency and order), reaching a compromise between costs and results. The cut-off frequency is chosen considering the receivers specifications: the diversity receiver [3] has 40 MHz of bandwidth at RF, whereas the auxiliary receiver [4] 30 MHz. However, the architecture presented in this work assumes a bandwidth of interest of 20 MHz at RF; after the downconversion, the signal is split in In-phase and Quadrature (I and Q) components, each with 10 MHz of bandwidth. Although the receivers are already equipped with 1st order baseband filters, in the addressed case they are not able to ensure a sufficient filtering of the noise. Therefore, the minimum f_c for the analog filters would be 10 MHz, but an higher cut-off frequency will be used, f_c = 15MHz; since these filters will be physically realized exploiting off-the-shelf components in order to carry out the experimental validation of the system, the aim is to ensure a certain margin in the system implementation and avoid signal distortion in the measurements. Regarding the design method, a low-pass Butterworth filter with flat pass-band frequency response is used: assuming unitary DC gain and considering the cut-off frequency where the filter gain is -3dB with respect to the DC value, the squared-magnitude filter response is defined as

$$\left|H(f)\right|^2 = \frac{1}{1+\left(f/f_c\right)^{2M}} \tag{2.42}$$

where M indicates the filter order. A Butterworth filter is characterized by a roll-off factor of -20·M dB/decade (Fig. 2.12a), hence the higher is the filter order, the sharper is the cut-off; with $M \to \infty$, the filter response becomes an ideal LPF, determining a Sinc function autocorrelation, as shown in Fig. 2.11. An analog Butterworth filter with finite order M produces an impulse response autocorrelation as reported in Fig. 2.12b; the analytic expression may be obtained by substituting the response (2.42) in (2.36) and computing the inverse Fourier transform. Even though it will affect the $x_f(t)$-$d_f(t)$ cross-correlation, and hence the DNR, in the addressed case it is not necessary to find the exact function but simply ensure an adequate filtering to

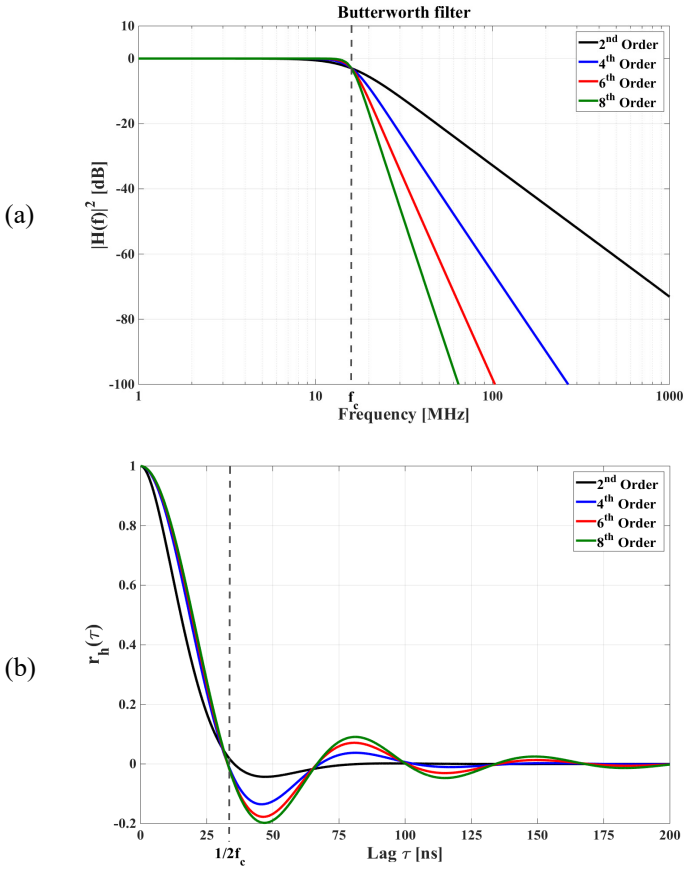

Figure 2.12: Squared-magnitude response (a) and normalized impulse response autocorrelation (b) of Butterworth filters for different orders, with f_c=15MHz

expand the dependence in the discrete time domain and make the digital equalizer able to work properly. The analog filters order will be chosen to ensure the desired noise reduction, verifying the results through simulations (next section). Regarding the digital equalizer, previously the theory of a N-order LMS FIR filter has been presented, but the sampling frequency f_s and the digital filter order N still need to be determined. These parameters are mutual dependent and clearly affect the performance of the digital path. The sampling frequency is related to the signal bandwidth, that is 10MHz single side band, but the cut-off frequency of the analog filters was fixed at f_c=15 MHz, hence f_s has to be $f_s > 2\ f_c$. It is worth to note that, with $f_s = 2\ f_c$ (Nyquist sampling frequency), the continuous-time autocorrelation (2.39) produces uncorrelated samples in digital domain, losing all the advantages of the analog filtering. Regarding the order of the filter equalizer, in common applications it depends on the complexity of the system response to be matched, but in the addressed case the effects of the antenna coupling can be easily equalized by controlling gain and delay of the reference signal. However, as described in depth, the limits are due to the signal uncorrelation, which was improved through filtering. Fixed the order of the analog filters, the higher is the sampling frequency, the higher will be the number of samples with a significant correlation; a digital filter with a higher order will be needed to exploit these samples thus improving the cancellation, to the detriment of a more expensive architecture.

2.3.5 System Requirements and Simulation Results

In order to prove the presented architecture as solution to restore the sensitivity of a SAW-less diversity receiver, the whole system has been modeled and simulated, identifying the requirements necessary to obtain a fair compromise between costs and performance. Since in this section only the performance of the digital path need to be verified to meet the desired noise reduction, diversity and the auxiliary path are supposed ideal, as well as the ADC. Initially, a 2nd order Butterworth filter with cut-off frequency f_c=15MHz is used before the ADCs, with

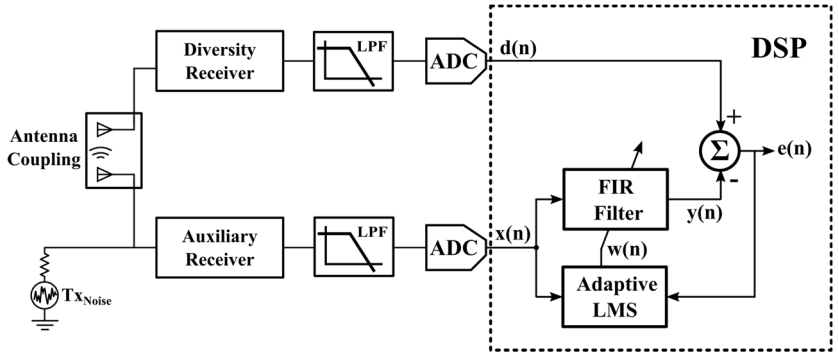

Figure 2.13: Proposed system overview, with digital equalizer based on LMS algorithm and analog LPF before ADC

a sampling frequency f_s=50MHz. As digital equalizer, a 4th-order complex LMS FIR filter will be used (Fig. 2.13), whose implementation has been reported in (2.28). The FIR filter order stems from considerations about the delay introduced by the antenna coupling, the sampling frequency and the signals correlation resulting from the analog filtering. With f_s=50MHz, the sampling period is t_s=20ns, and the coupling delay γ, that is about 3-4ns, is only a fraction of t_s. Regarding the signal correlation, even if an ideal LPF was used, with these sampling and cut-off frequency about two samples per lobe from the Sinc function (Fig. 2.12b) are acquired; therefore, exploiting the first four samples is sufficient, since the samples belonging to the first two lobes show the most significant correlation. Therefore, the noise reduction results obtained in this first configuration are reported in Fig. 2.14. The first one (Fig. 2.14a) shows the DNR as function of the coupling delay: considering the total band [$-f_s$,$+f_s$], the comparison between the Wiener (ideal) and the LMS (real) equalizer proves that the performance degradation introduced by the LMS approximation are essentially negligible, reaching almost the same DNR of an ideal Wiener filter. For example, with a delay of 4ns, the theoretical noise reduction is 11.32 dB, whereas the LMS reaches 11.26 dB, a rather negligible difference. It is well known that the step-size μ in (2.28) affects the performance of the LMS algorithm: a small μ allows to minimize the misadjustment, to the detriment of a slower convergence. However, in the proposed application, the convergence time is not a

(a)

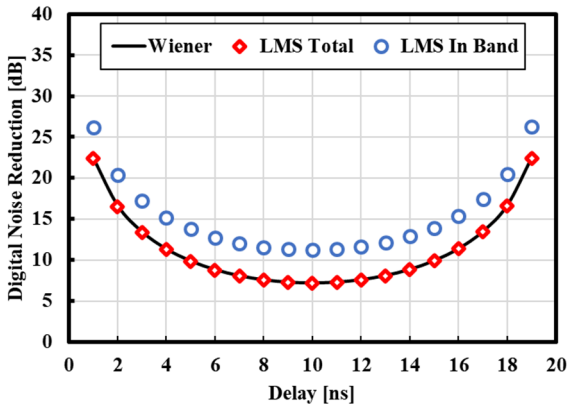

(b)

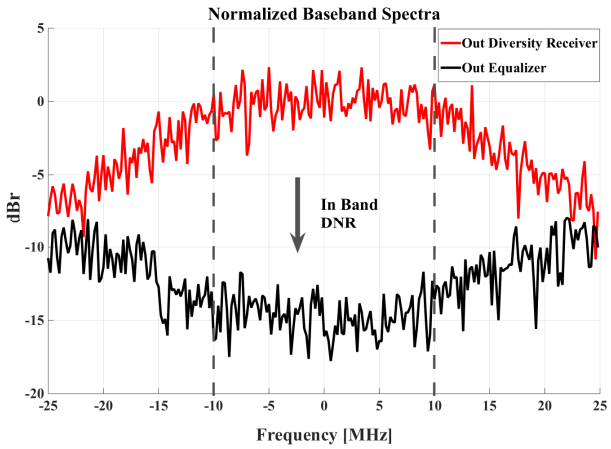

Figure 2.14: Digital noise reduction with 2nd order analog filter (f_c=15MHz) and f_s=50MHz, (a) versus group delay for ideal Wiener (line) and realistic LMS (diamonds) equalizer considering the whole bandwidth ± f_s and the band of interest ±10MHz (circles); (b) example of resulting spectra with delay γ=4ns

limit, since the equalizer has to follow the antenna coupling variations due to the interactions with the external environment, which are inherently much slower than the rate of convergence of the digital path, as it will be proved by the experimental results in Section 2.4. Figure 2.14a also shows the in band DNR, that is the reduction in the band of interest [-10MHz,+10MHz] achieved with the LMS equalizer. An example of resulting spectra, normalized on the power of the signal at the output of the diversity receiver, with a delay of 4ns, is reported in Fig. 2.15b, where the in band reduction is highlighted. Even though it

has been shown the DNR for different delays in the range of the sampling period, it is worth to note that a realistic group delay is about 3-4ns in the addressed case, and hence these values will be considered to evaluate the equalizer performance. However, for γ=4ns, a DNR=15.2dB is achieved in this configuration, too low compared with the desired DNR, that is at least 28dB. In order to improve the equalizer performance, a 4th order Butterworth filter with cut-off frequency f_c=15MHz is now used, with a sampling frequency f_s=50MHz; the digital equalizer is a 4th order LMS FIR filter, like before. An analog filter with a higher order allows to further extend the correlation (Fig. 2.12), involving a larger number of samples and making the equalization process more effective; indeed, as shown in Fig. 2.15, the same digital equalizer is now able to reach a higher DNR. For example, still considering γ=4ns, the in band DNR is about 36dB, exceeding the desired performance. Therefore, in this configuration, the proposed method is able to ensure the desired performance determined in Section 2.2.2; it is worth to recall that the required DNR was computed so that the residual Tx noise after the cancellation gives rise to a further NF degradation of the diversity receiver negligible (≤0.1dB in the worst case) if compared with the degradation due to the auxiliary receiver

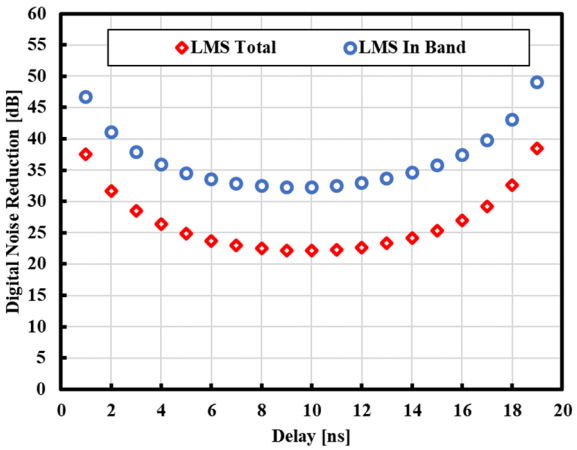

Figure 2.15: Digital noise reduction with 4th order analog filter (f_c=15MHz) and f_s=50MHz versus group delay, considering the whole bandwidth ±f_s (diamonds) and the band of interest ±10MHz (circles)

(a)

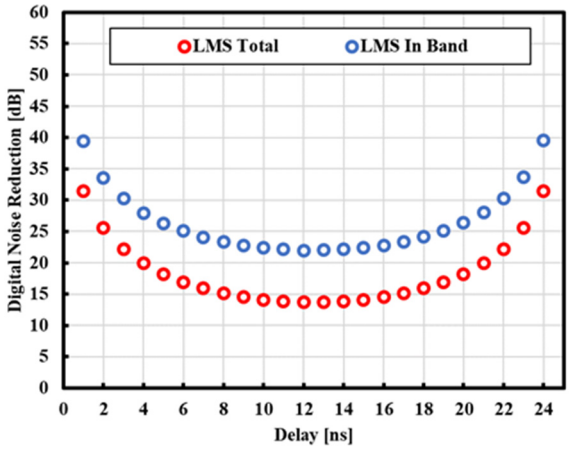

(b)

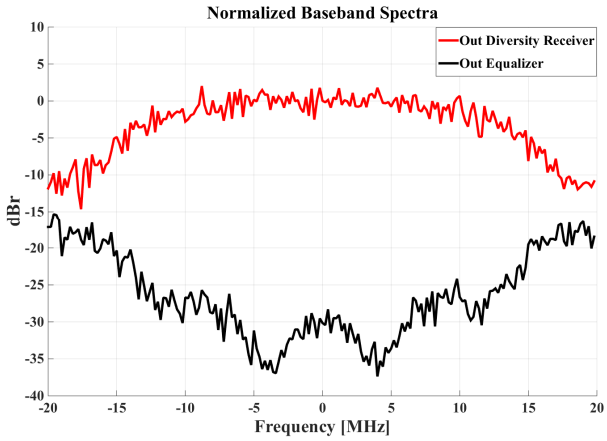

Figure 2.16: Digital noise reduction with 4th order analog filter (f_c=15MHz) and f_s=40MHz, (a) versus group delay considering the whole bandwidth $\pm f_s$ (diamonds) and the band of interest ±10MHz (circles); (b) spectra with delay γ=4ns

noise. Since there is a considerable difference between the obtained results and the required DNR, in the last configuration the sampling frequency will be lowered from 50 to 40MHz, with the aim of reducing the overall costs of the implemented architecture. As shown in Fig. 2.16, although the DNR is lower than the previous case, for γ=4ns it is about 28dB, meeting the requirements. The resulting steady-state digital filter response is reported in Fig. 2.17: assuming the system configuration described in Tab. 2.1, the gain (Fig. 2.17a) to be matched can be computed from (2.9), where the attenuation *Att* is obtained from

(a)

(b)

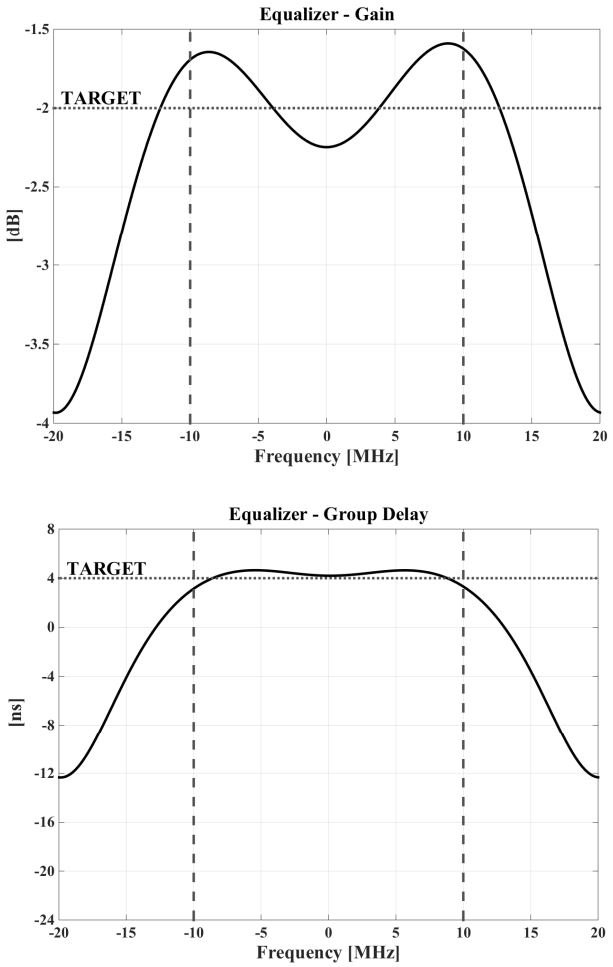

Figure 2.17: Digital equalizer response, (a) gain G_{eq} from (2.9) and (b) group delay with γ=4ns

(2.5), whereas the group delay (Fig. 2.17b) of the digital filter matches the 4ns of delay introduced by the antenna coupling. It is possible to note that, in the band of interest, the equalizer ensures a good approximation of the desired response. Until now, the proposed architecture (Fig. 2.3) has been tested considering as signal of interest the Tx noise which falls in the Rx band, and completely ignoring the real desired signal in reception. This external signal, being completely uncorrelated with the local Tx noise, does not compromise the system performance. As introduced in Section 2.2.2, in the worst case

(transmitter at full power) the presented system improves the diversity receiver sensitivity, degraded by the Tx noise, of about 11 dB if compared with the worsening that would be verified without DNR. In order to prove that the equalizer is not affected by the desired signal, it is tested in the presence of a 20 MHz QPSK signal, and the results are shown in Fig. 2.18. Assuming a received signal power such that the resulting Modulation Error Ratio (MER) is 2dB when corrupted by the unfiltered Tx noise (i.e. without the DNR), after the equalization the MER is 13dB, proving the expecting improvement of 11dB. In this case the total noise (Fig. 2.18a) takes into account the diversity receiver noise and the slight worsening (about 1.1dB) due to the auxiliary

(a)

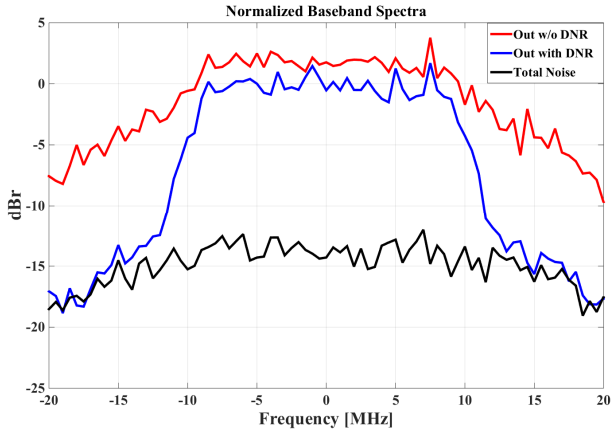

(b)

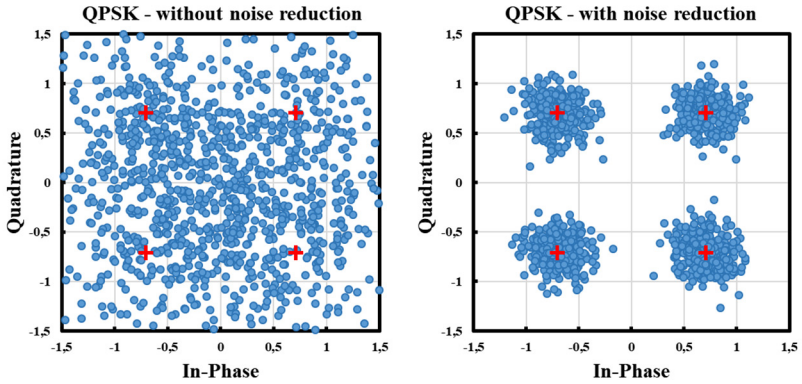

Figure 2.18: Digital equalization tested in presence of a 20 MHz QPSK received signal, (a) normalized spectra, (b) constellations without and with DNR

TABLE 2.2
SUMMARY BASEBAND SPECIFICATIONS

Analog LPF	4^{th} order Butterworth f_c = 15MHz
ADC	f_s = 40MHz 8bits
Digital Equalizer	4^{th} order complex LMS FIR filter

receiver noise and the residual Tx noise after the cancellation. Regarding the analog to digital conversion, it has been assumed so far as an ideal sampling, only characterized by the sampling frequency; however, some considerations about the quantization noise effects are needed. The required number of bits may be estimated considering the noise ratio given by (2.7) for the auxiliary receiver and (2.8) for the diversity receiver; however, for the presented application, the aim of avoiding further degradation of the receiver sensitivity leads to assume a larger dynamic range. Therefore, if at least 28dB of noise reduction are needed, the required dynamic range is 6 bits but, in order to not compromise the performance of the digital path, 8 bits would be ideal. The baseband system specifications are summarized in Tab. 2.2.

2.4 Experimental Measurements

The complete architecture is implemented and tested to experimentally prove its performance; a diagram of the measurement setup is shown in Fig. 2.19. The auxiliary receiver chip [4] and the diversity receiver chip [3] are bonded on Printed Circuit boards (PCB), whereas two boards, with low-pass filters and ADCs, define the interface between the RF and the digital path. These boards are designed with the requirements reported in Tab. 2.2 and realized using off-the-shelf components. The digital equalizer is implemented on a Cyclone IV EP4CE115F29C7 Altera FPGA, which also provides the signal clock to the ADCs boards.

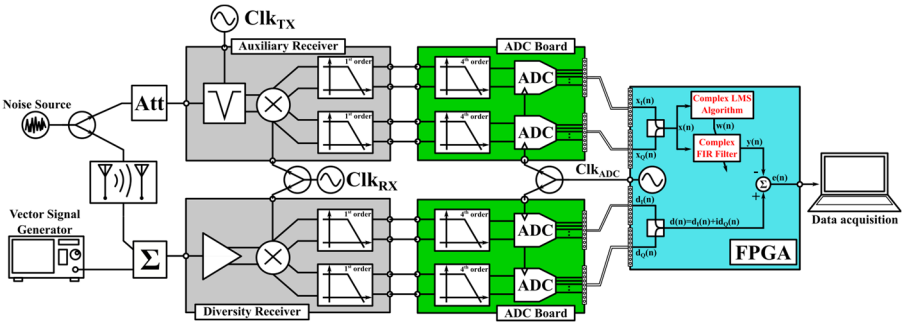

Figure 2.19: Measurement setup

The processed data are acquired in real-time from the FPGA through the SignalTap II Logic Analyzer Tool of Quartus and analyzed on MatLab. An external generator provides the Tx clock to the notch filter of the auxiliary receiver, whereas another external generator provides the same Rx clock to the mixers of both receivers, in order to down convert the same Rx band. Finally, a vector signal generator produces the desired Rx signal at the input of the diversity receiver, whereas a noise source allows to reproduce the broadband Tx noise at the input of both receivers. On the basis of the components available in the laboratory, the system is tested with Clk_{TX}=1GHz and Clk_{Rx}=1.2GHz, even though the receivers can operate at higher frequencies, whereas $Clk_{ADC}=f_s$=40MHz. Regarding the antenna coupling, since there are not available PIFAs able to work at 1.2GHz, it is reproduced employing a RF attenuator and a transmission line properly designed, whose

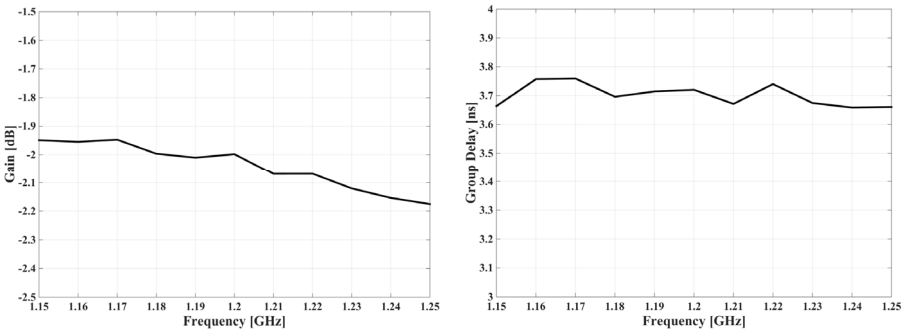

(a) (b)

Figure 2.20: Measured parameters of transmission line, (a) gain and (b) group delay, designed to model the antenna coupling

measurements are shown in Fig. 2.20. The transmission line ensures ≈-2dB of gain (Fig. 2.20a) and a group delay of about 3.7ns (Fig. 2.20b) across 100MHz bandwidth at 1.2GHz; additional 23dB of RF attenuation are added to achieve *CP*=25dB. Figure 2.21 schematizes the digital path implemented on FPGA (Fig. 2.19). Some low-pass FIR filters with 10MHz of bandwidth are used in front of the equalizer to remove out-of-band spurious emissions, generated by the ADC boards, from the I and Q components provided by the receivers. It is worth to recall that these digital filters cannot improve the cross-correlation between the processed signals and hence the performance of the equalizer. After the FIR filters, the signal processing is represented in complex form, as described in (2.28), with the reference signal $x(n)=x_I(n)+ix_Q(n)$ constituted by the I and Q components from the auxiliary and equivalently the desired signal $d(n)=d_I(n)+id_Q(n)$ from the diversity receiver. The effective implementation of the algorithm, obtained by decomposing the complex form (2.28), is

$$y(n) = y_I(n) + iy_Q(n) = \left(\mathbf{w}_I^T\mathbf{x}_I + \mathbf{w}_Q^T\mathbf{x}_Q\right) + i\left(\mathbf{w}_I^T\mathbf{x}_Q + \mathbf{w}_I^T\mathbf{x}_Q\right)$$

$$\varepsilon(n) = \varepsilon_I(n) + i\varepsilon_Q(n) = \left(d_I(n) - y_I(n)\right) + i\left(d_Q(n) - y_Q(n)\right)$$

$$\mathbf{w}(n+1) = \mathbf{w}(n) + \mu\varepsilon(n)^*\mathbf{x}(n) = \tag{2.43}$$

$$= \left[\mathbf{w}_I(n) + \mu\left(\varepsilon_I(n)\mathbf{x}_I(n) + \varepsilon_Q(n)\mathbf{x}_Q(n)\right)\right] +$$

$$+ i\left[\mathbf{w}_Q(n) + \mu\left(\varepsilon_I(n)\mathbf{x}_Q(n) - \varepsilon_Q(n)\mathbf{x}_I(n)\right)\right]$$

where $\mathbf{w}(n)=\mathbf{w}_I(n)+i\mathbf{w}_Q(n)$ represent the adaptive complex coefficients of equalizer. In order to validate the proposed architecture, it is tested in the same configuration reported in Section 2.2.2 (summary in Tab. 2.1). Figure 2.22a reports the NF degradation (measured and calculated) of the diversity receiver as function of the transmitter power. Considering that the noise source generates an equivalent noise power

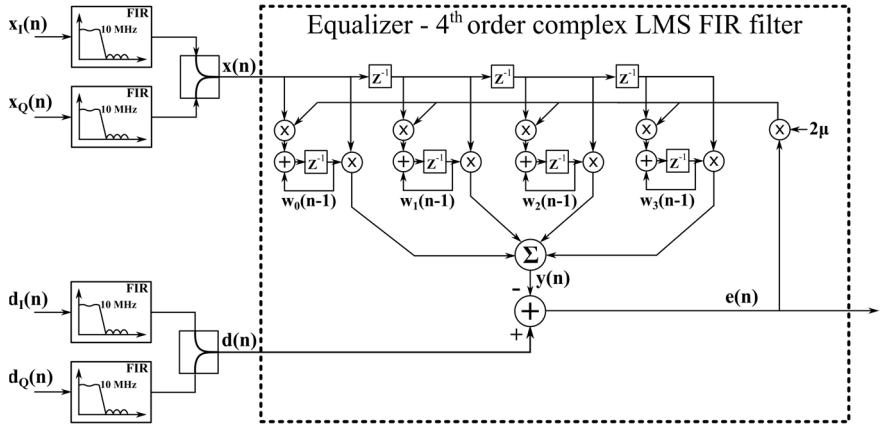

Figure 2.21: Digital path implemented on FPGA

P_{Txn} = -154dBc/Hz, which corresponds to a Tx noise at the input of the diversity receiver equal to $P_{Txn,Rx}$ = -156 dBm/Hz (2.2) in the worst case (P_{TX}=23dBm), the resulting NF degradation (2.4) $\Delta NF_{Txn} \approx$ 13dB (assuming NF_{Rx} = 5.2dB). With the proposed architecture, the digital noise reduction ensures a sensitivity degradation (2.15) $\Delta NF_{Tot} \approx$ 1.1dB, with an effective noise reduction of ≈12dB (even though more than 28dB of Tx noise reduction are achieved through the digital equalization, as it will be shown later). In both cases, the measurements are in good agreement with the theoretical trends. Figure 2.22b shows the resulting double side band spectra (with and without DNR) normalized on the NF_{Rx}, with P_{TX}=23dBm. As demonstrated in Section 2.3.5, in this configuration the digital equalizer should ensure about 28dB of Tx noise reduction in 20MHz of bandwidth; however, it is quite difficult to directly measure the Tx noise reduction in this experimental setup, being the residual noise given by the diversity receiver noise plus the degradation due to the auxiliary receiver NF and the Tx noise after the cancellation. Therefore, the DNR is estimated by increasing the noise power P_{Txn} (with P_{TX}=23dBm) and measuring the resulting NF degradation ΔNF_{Tot} and the effective noise reduction; the results are shown in Fig. 2.23, where the theoretical results, supposing DNR=29dB, are compared with the measurements. Fig. 2.23a shows the ΔNF_{Tot} as function of the noise power: with a fixed DNR, the higher is the noise level, the higher will be the residual signal after the

cancellation and hence its contribute ΔNF_{DNR} to the total NF degradation. Moreover, the effective noise reduction (Fig. 2.23b) is also measured and compared with the calculated results, still assuming a DNR=29dB: increasing P_{Txn}, the Tx noise is not completely removed due to the limited DNR and the effective noise reduction converges toward 29 dB for high input noise. Both experiments show good agreement between measurements and theoretical results, thus confirming the assumption DNR=29dB and the desired performance of the equalizer. Testing the system up to P_{Txn} = -143dBc/Hz also proved

(a)

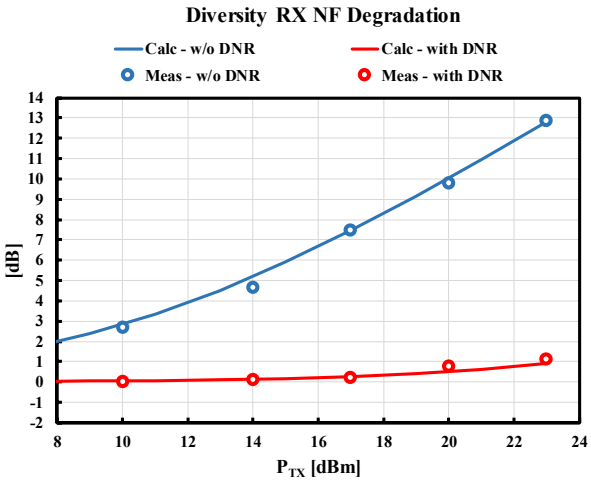

(b)

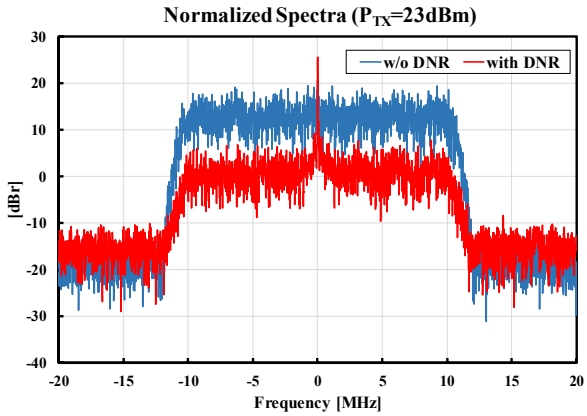

Figure 2.22: (a) Measured (circles) and calculated (lines) NF degradation versus Tx power, with and without DNR; (b) measured normalized spectra with Tx at full power

that the proposed architecture can manage higher Tx noise level with a reasonable sensitivity degradation, even though a lower reference Tx noise P_{Txn} = -155dBc/Hz was assumed in the previous sections. In that case the desired DNR=28dB allowed to limit the NF degradation due to the finite cancellation ($\Delta NF_{DNR} \approx 0.1$dB) and hence the total degradation ($\Delta NF_{Tot} \approx 1.1$dB); clearly, a higher Tx noise produces a higher ΔNF_{Tot} (≈ 2.05dB with P_{Txn} = -143dBc/Hz), which however can be reduced by improving the DNR, for example raising the sampling frequency as demonstrated in Section 2.3.5. Regarding the convergence time of the equalizer, it was previously assumed that it is not a limit, since the

(a)

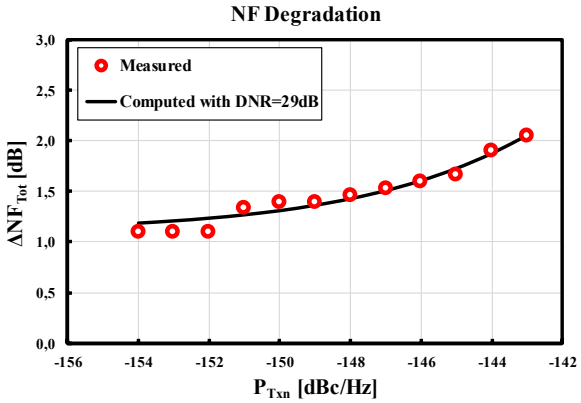

(b)

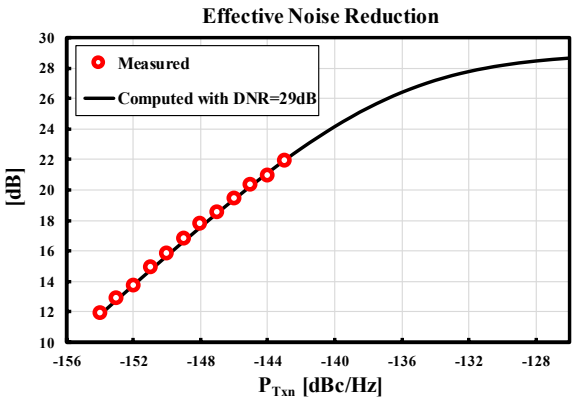

Figure 2.23: (a) Measured (circles) and calculated (line, assuming DNR=29dB) NF degradation ΔNF_{DNR} versus Tx noise power; (b) measured (circles) and calculated (line, assuming DNR=29dB) effective noise reduction versus Tx noise power

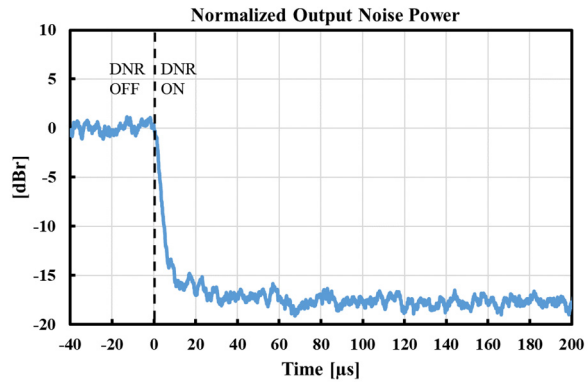

Figure 2.24: Measured time waveform of the output equalizer (P_{Txn} = -147dBc/Hz and steady-state effective noise reduction of 18.1dB)

variation rate of the antenna coupling is inherently mush slower, being due to the interactions with the external environment. For example, in [12] it is shown that a PIFA antenna in handheld device can exhibit significant temporal variations in the order of milliseconds. The time waveform reported in Fig. 2.24 prove that the digital equalizer, tested with P_{Txn} = -147dBc/Hz, is able to reach the optimal configuration (steady-state effective noise reduction of 18.1dB) after a few tens of microseconds, thus ensuring an efficient tracking of the antenna variations that occur during normal functioning of the device. Finally, the equalizer is tested with a 20 MHz QPSK modulated signal placed at the input of the diversity receiver, which represents the desired signal in a realistic implementation of the system. The resulting constellations, with a without digital noise reduction, are shown in Fig. 2.25.

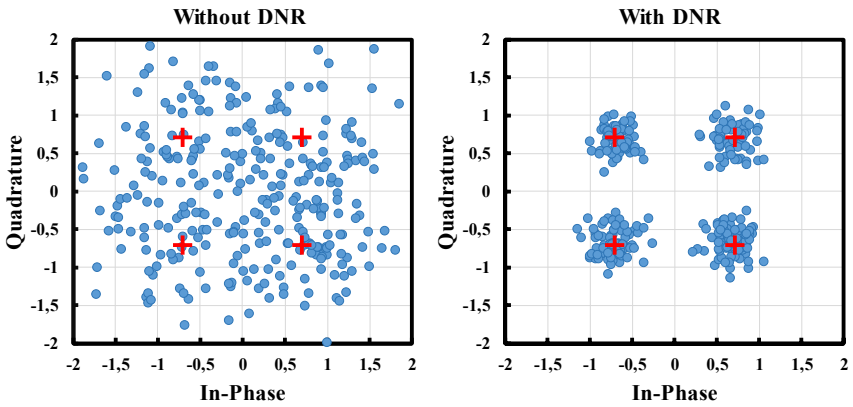

Figure 2.25: Measured constellations with a 20MHz QPSK modulated signal at the input of the diversity receiver

Chapter 3

Digital Background Control for Hybrid Transformer-based Receivers

In this Chapter, the design and hardware implementation of a digital control system tailored to a hybrid transformer-based duplexer is proposed. Working at Nyquist sampling frequency, it finds the optimal transmit-receive isolation in about 150 µs even when modulated signals with high PAPR (16-QAM) are transmitted. Section 3.1 proposes an overview of the state of the art. Section 3.2 briefly introduces the HT-based duplexer and the isolation sensitivity. Section 3.3 describes the complete control algorithm. In Section 3.4, a deep analysis of the control system performance is carried out. Finally, Section 3.5 deals with the hardware implementation and Section 3.6 shows the experimental measurements.

3.1 SAW-less Duplexers: State-of-the-Art

Commercial radios rely on highly selective off-chip SAW filters to eliminate large out-of-band blockers. SAW-based duplexers are used in FDD applications, to provide transmitter-to-receiver isolation (ISO_{TX-RX}) in excess of 50 dB and relax the receiver linearity requirements. Several solutions have been recently proposed to replace the multiple off-chip duplexers, each operating on a single band, with a single reconfigurable component, thus reducing system cost, complexity and area. In [13] a series stacked transformer combines transmitter and receiver and an RF current DAC in shunt with the receiver cancels the transmit signal leakage and creates a virtual ground across the receiver, preserving the transmitter efficiency and providing 50 dB ISO_{TX-RX}. The transmit power however is limited to less than 13 dBm and the canceler consumes 60 mW. In [14] an artificial transmission-line is used

to realize selectivity through constructive/destructive interference but ISO_{TX-RX} is only 23 dB. An N-path based filter further reduces transmitter noise injection into the receiver but its effectiveness reduces at high transmit power levels due to nonlinear effects, degrading the receiver noise figure. The hybrid transformer (HT) has also been proposed in various configurations [2], [6], [15], [16], [19] to replace SAW-based duplexers. Even though a 3-dB loss both in TX-antenna and antenna-RX paths is suffered, its high linearity makes it the most suitable solution for high TX power systems. Furthermore, the HT could be used as an integrated antenna interface in future full-duplex transceiver architectures [17], [18]. The HT is fully passive and, contrary to SAW-based duplexers where isolation is guaranteed through filtering, in HT-based duplexers isolation is based on matching between the antenna impedance with an on-chip programmable balancing impedance. One of the main issues of HT-based duplexers is the sensitivity of ISO_{TX-RX} to the antenna impedance. In fact, the antenna impedance changes rapidly with frequency and it slowly varies with time due to interactions with the surrounding environment. In order to deal with antenna impedance frequency variations, the balancing impedance must be able to cover a large impedance range with sufficient resolution. Moreover, a low-power antenna monitoring system is required to automatically and adaptively adjust the balancing to follow the antenna impedance time variations. Complex balancing impedance architectures able to ensure high isolation levels in more than one band [6], [15] and [16] (e.g. TX and RX bands for FDD) or in wide bandwidths [18] have been reported. Nevertheless, full integration of the complete system, including the real-time control loop, has not yet been reported in the literature. In fact, increasing the complexity of the balancing impedance and/or adding more control variables, may allow to cover a larger impedance range with greater resolution but it would also make the design of the real-time balancing impedance control circuitry and optimization algorithm more difficult. It should be able to find the initial balancing configuration which maximizes the isolation level and then, through a background control, to track the variations of

the antenna impedance without interfering with the normal operations of the transceiver.

3.1.1 Control Algorithms: State-of-the-Art

Several works prove that relevant antenna impedance variations occur on a time scale of a few milliseconds (e.g. >10 ms in [12]). Hence, to ensure static conditions, the optimization process should be performed in a sufficiently small time (e.g. ≈100 μs). The solutions in [5], [17] and [18] are, to the best of the authors knowledge, the most complete architectures proposed so far. In [17] only the HT and impedance balancing network were integrated on the same chip, whereas a commercial reconfigurable radio platform was used for the measurements and the control algorithm, based on a mixed deterministic/iterative approach tailored to a full-duplex transceiver prototype, was implemented in software. A long initial training phase is used to build an analytical model of the HT+balancing impedance prototype with a fixed antenna impedance. Then, a training sequence with a relatively small number of steps allows to determine the optimal balancing impedance settings. This method is well-suited for packet-based standards (e.g. IEEE 802.11) but, to initiate the iterative phase, a known balancing impedance condition must be restored first, which momentarily degrades the isolation level. Hence it cannot be generally applied to different standards. Moreover, this method is not able to track varying temperature and operating conditions, that inevitably degrade the precision of the model parameters. Hence, to maintain a good isolation, the training sequence must be repeated, potentially leading to recurring service interruption. In [18] off-the-shelf parts, including an automated impedance tuner, were used to test the proposed control algorithm, which was implemented in software. It relies on a deterministic balancing algorithm derived from an analytical modeling of the self-interference function in HT-based duplexers. According to the authors, this control algorithm allows to find the best balancing combination with a fewer number of measurements if compared with an iterative method, reducing the overall convergence time at the price

of a significantly increased hardware complexity (a very large number of operations, including nonlinear ones, are required). Moreover, as highlighted by the authors, a very high measurement SNR is required to achieve the desired isolation. For 50 dB isolation, a minimum SNR of 40 dB is necessary at the receiver output. This was easily achievable in the test setup in [18], based on the off-the-shelf components, but it would have represented a bottleneck if the system had been implemented in an IC prototype. Therefore, in [17] and [18] the tuning algorithms have been only tested in software, without carefully analyzing the overhead introduced by their hardware implementation, and an experimental validation of the complete system in real-time was not reported. In [5] an iterative digital control algorithm was designed to provide a feasible real-time control of the $ISO_{TX\text{-}RX}$ level for the receiver [2], in which the HT, the balancing impedance and the receiver were integrated in a single chip. The system was implemented in a FPGA, demonstrating fast convergence time and minimal RF front-end overhead. Figure 3.1 depicts the block diagram of the complete system, which includes the HT-based receiver, the digital control system and two analog-to-digital converters (ADCs) at the interface. Due to the high linearity of the receiver, $ISO_{TX\text{-}RX}$ requirements are relatively relaxed to only 45 dB, enabling the use of a simple balancing impedance, based on an array of parallel switched resistors and capacitors. Although the measurements were carried out using the main receiver tuned at the TX carrier frequency for TX leakage measurement,

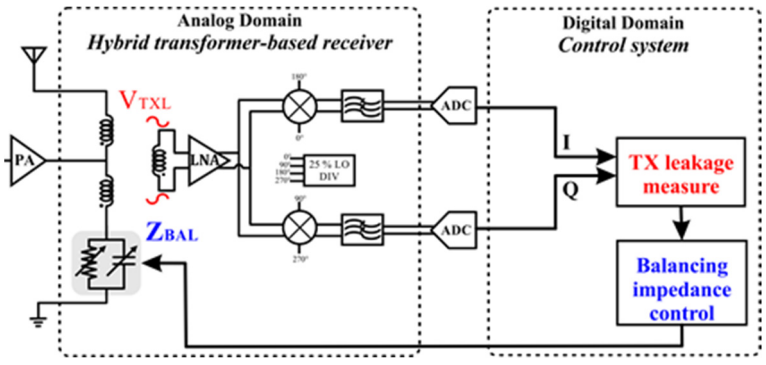

Figure 3.1: Complete system overview: the HT-based receiver is the RF chip prototype [2], whereas the control system is described in this work

an auxiliary receiver with much relaxed performances, can be used to perform this function, while still meeting the isolation and convergence time requirements with margin. The use of an iterative approach, based on real-time measurements, allows to reduce the computational complexity; however, in order to keep the number of iterations and therefore the convergence time under control, an adaptive algorithm was implemented. The system was tested with a sinusoidal signal, which is not adequate to realize a real-time background control, and the analysis presented in this work shows that the use of a modulated test signal degrades unacceptably the convergence time of the algorithm in [5]. Table 3.1 summarizes the differences between the proposed solution and previous works. An improved digital control, compatible with modulated test signals and able to work without interfering with

TABLE 3.1
COMPARISON WITH STATE-OF-THE-ART CONTROL ALGORITHMS

	This Work	ICECS [5]	5GU [17]	TCAS II [18]
Receiver	IC Prototype [2]	IC Prototype [2]	Warp v3	PXIe VST
Duplexer	IC Prototype [2]	IC Prototype [2]	IC Prototype	Commercial HTs
Control Algorithm	Iterative	Iterative	Deterministic + Iterative.	Deterministic (Modelling)
Complexity	LOW	LOW	MEDIUM	HIGH
Algorithm Implementation	Hardware (FPGA)	Hardware (FPGA)	Software (MatLab)	Software (LabView)
Real-time Operations	YES	YES	NO	NO
Test Signal / Standard	WCDMA / 3G	Sine Wave	IEEE 802.11 - STS	OFDMA LTE
Convergence time	50 µs (Sinewave) [1]	80 µs (Sinewave) [1]	~100 µs (Determ.) + ~100 µs (Iterative)	N/A
	153 µs (16-QAM) [1]	350 µs (16-QAM) [2]		

[1] Measurement results [2] Simulation only (computed in this work)

the normal transceiver operations and with a minimal system overhead will be presented and experimentally validated in next sections; the limitations of the approach proposed in [5] when a modulated signal is used will be highlighted, and an enhanced adaptive algorithm proposed. It will enable 2.5x faster optimization in the most critical case, when modulated signals with high Peak to Average Power Ratio (PAPR) are transmitted, making the complete system suitable for a SAW-less mobile transceiver.

3.2 Hybrid Transformer-Based Duplexer

An HT is a passive four-port network that can be designed to split the power from any of the four ports into two other ports while no power is delivered to the fourth (isolated) port. These properties can be exploited in the context of an FDD transceiver to implement an on-chip tunable duplexer. A possible configuration, corresponding to the one adopted in [2], is reported in Fig. 3.2: two coupled inductors are connected in series with each other, forming an auto-transformer. Each inductor terminal represents a port with respect to a common ground reference. The center-tap of the auto-transformer is the TX port, driven by the power amplifier (PA), while the other two terminals correspond to

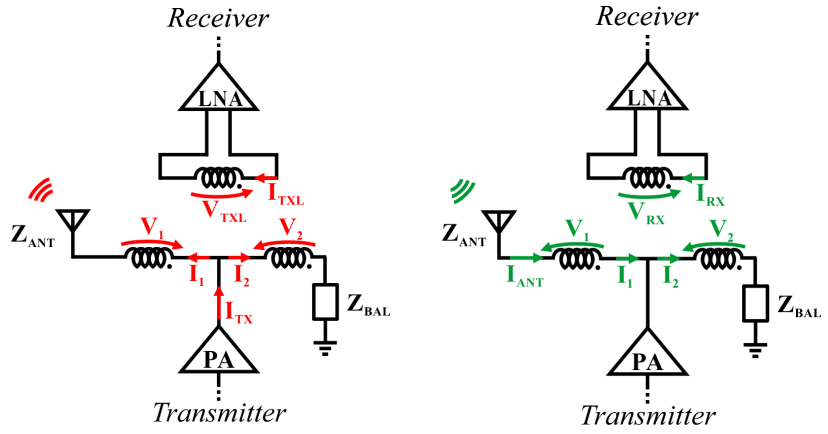

Figure 3.2: Theoretical behavior of an ideal HT-based duplexer in (a) transmission and (b) reception mode

antenna and balancing impedance port. The two windings forming the auto-transformer (primary windings) are coupled to a third coil (secondary winding), whose two terminals define the fourth (differential) port, i.e. the RX port, connected to the low-noise amplifier (LNA). The HT ideal operation can be easily understood considering the *symmetrical* HT, where the two windings forming the auto-transformer are equal. In the receive mode, the received signal from the antenna produces a current which flows through the primary windings in the same direction, generating a net magnetic flux that gets coupled to the RX port. In transmission mode, the PA supplies the current at the center-tap of the auto-transformer, where it splits between the antenna and the balancing impedance paths. With equal antenna Z_{ANT} and balancing impedance, $Z_{ANT} = Z_{BAL}$, equal and opposite magnetic fluxes on the primary windings are generated, inducing zero current on the secondary winding of the transformer. In this way, the transmitted power is split equally between antenna and balancing impedance and the LNA is perfectly isolated. In practice, perfect matching between Z_{ANT} and Z_{BAL} cannot be ensured since Z_{ANT} will vary with frequency and time and Z_{BAL} can be controlled with finite resolution, leading to a finite $ISO_{TX\text{-}RX}$. Isolation may be defined as [19]

$$ISO_{TX-RX} = \frac{V_{TXL}}{V_{TX}} \propto \left| \left(\frac{Z_{ANT} - Z_{BAL}}{Z_{ANT} + Z_{BAL}} \right) \right| \tag{3.1}$$

The balancing impedance should match the antenna impedance over the bandwidth of the transmitted signal. Moreover, the antenna impedance is perturbed by external environment (e.g. objects, human body, etc.), hence it can exhibit significant variations in time domain [12]. The TX-RX isolation level as described in (3.1) is reported in Fig. 3.3, assuming static conditions. In the proposed architecture, the balancing impedance is realized with a digitally-controlled R-C parallel network: the variable real part covers a range of 35-70 Ω with precision of 0.14 Ω, implemented with an 8-bit binary array of parallel programmable resistors. In order to cover both positive and negative reactive antenna impedances, two arrays of variable capacitors are used, one at the

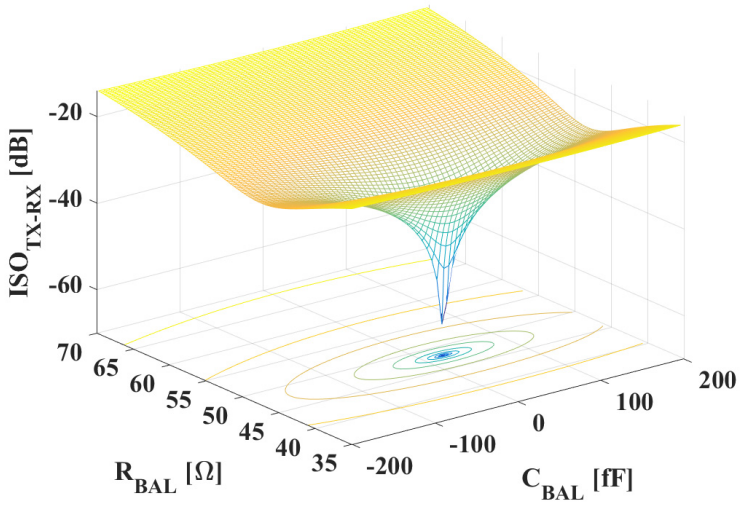

Figure 3.3: TX-RX isolation level as a function of Z_{BAL} (for a given Z_{ANT}) computed with the formula (3.1)

antenna port, to compensate for inductive antenna impedances, and one at the balancing port. The resulting effective balancing capacitance is the difference between the two. Each variable capacitor covers the range 200-400 fF with a precision of 6 fF, and consists of a 5-bit binary array. The chosen range is similar to the one adopted in prior works [16], even though a larger range in the reactive part would be desirable to cover practical antenna realizations.

3.3 Control System Design

Although the previous analysis of the HT is actually valid only in ideal conditions (lossless transformer, unitary coupling factors, etc.), it is adequate for the purpose of designing the control system. For a given antenna impedance, which is a priori unknown and time-dependent, the tuning system, through real-time measurements of the TX leakage power in the HT receiver port, searches the best balancing impedance value which maximizes the $ISO_{TX\text{-}RX}$ at the transmitted frequency. The maximization of the isolation level is obviously equivalent to the

minimization of the TX leakage signal P_{TXL} in the receiver path. Assuming that the receiver local oscillator (LO) is tuned to the transmit carrier frequency, and that no other signal is being received by the antenna, the P_{TXL} is estimated as

$$P_{TXL}(Z_{BAL}) = I^2(Z_{BAL}) + Q^2(Z_{BAL}) \tag{3.2}$$

It is possible to define an optimization problem as follows

$$\min_{Z_{BAL}} P_{TXL}(Z_{BAL}) \qquad Z_{BAL} = [R_{BAL}, C_{BAL}]$$

$$R_{BAL} \in \left[\min(R_{BAL}), \max(R_{BAL})\right] \quad \Delta R_{BAL} = \frac{\max(R_{BAL}) - \min(R_{BAL})}{2^{B_1}} \tag{3.3}$$

$$C_{BAL} \in \left[\min(C_{BAL}), \max(C_{BAL})\right] \quad \Delta C_{BAL} = \frac{\max(C_{BAL}) - \min(C_{BAL})}{2^{B_2}}$$

where range and resolution of resistance and capacitance of the digitally controlled balancing impedance are defined, whereas $B_1 = 8$ and $B_2 = 6$ (given by the two 5-bit array of capacitors) indicate the number of bits on which these variables are represented. As well known, there are several methods and algorithms to solve an optimization problem, mainly distinguished in terms of complexity, robustness and convergence time. Given the simple balancing impedance structure adopted in this work, the optimization problem is quite simple (a two-dimensional discrete optimization problem with a single global minimum, as shown in Fig. 3.3), and the goal is to achieve a low-cost control system. In the solutions [17], [18] the tuning algorithms exploit complex HT models (analytic or estimated through system training), but these solutions would require a challenging hardware implementation. Among the most well-known optimization methods, different solutions have been investigated to find the algorithm with a fair trade-off between performance and simplicity, and some gradient-based iterative algorithms have been analyzed. In optimization problems, *Newton's methods* [21] exploit both first and second derivatives of the objective function to find the optimum value, however in this work they are not available and too expensive to be estimated with an appropriate precision (in particular the second

derivatives). Therefore, a simple *gradient descent method* [21] has been investigated as starting point of the control system, and a *customized gradient descent method* will be proposed.

3.3.1 Optimization Phase

The optimization phase (or coarse search) is carried out at startup of the system or after a major change in the operating conditions (e.g. a change in the transmission band), in order to find the best balancing condition of the HT starting from a totally unknown state. To solve the problem (3.3) implementing the standard *gradient descent method*, the optimization algorithm can be defined as follows

$$Z_{BAL}^{(n+1)} = Z_{BAL}^{(n)} - \boldsymbol{\gamma}^{(n)} \nabla P_{TXL}\left(Z_{BAL}^{(n)}\right) \quad n \geq 0 \tag{3.4}$$

where n indicates the iteration number and $\boldsymbol{\gamma}$ the updating step size. However, it is necessary to make a few preliminary remarks: the objective function P_{TXL} is a priori unknown, as its gradient; the solutions domain (i.e. the balancing impedance range) is discrete; the standard gradient method usually shows a slow convergence around the optimum point. An estimation of the gradient components can be obtained by measuring the signal P_{TXL} and exploiting finite difference approximation (e.g. forward difference), which obviously will be afflicted by a certain error due to the approximation and the signal noise. Therefore, to improve the control system noise immunity and further simplify the algorithm implementation, only the difference sign will be used to identify the direction toward which the balancing impedance should move in order to minimize the TX leakage power. Hence, the problem (3.4) becomes

$$Z_{BAL}^{(n+1)} = Z_{BAL}^{(n)} - \boldsymbol{\gamma}^{(n)} sgn\left(\nabla P_{TXL}\left(Z_{BAL}^{(n)}\right)\right) \quad n \geq 0 \tag{3.5}$$

where

$$\begin{aligned}&\operatorname{sgn}\left(\nabla P_{TXL}\left(Z_{BAL}^{(n)}\right)\right)\approx\\&\approx \operatorname{sgn}\left(dif_R P_{TXL}\left(Z_{BAL}^{(n)}\right)\right)\hat{R}_{BAL}+\operatorname{sgn}\left(dif_C P_{TXL}\left(Z_{BAL}^{(n)}\right)\right)\hat{C}_{BAL}\end{aligned} \tag{3.6}$$

and

$$\begin{aligned}dif_R P_{TXL}\left(Z_{BAL}^{(n)}\right)&=P_{TXL}\left(\left[R_{BAL}^{(n)}+\Delta R_{BAL},C_{BAL}^{(n)}\right]\right)-P_{TXL}\left(\left[R_{BAL}^{(n)},C_{BAL}^{(n)}\right]\right)\\dif_C P_{TXL}\left(Z_{BAL}^{(n)}\right)&=P_{TXL}\left(\left[R_{BAL}^{(n)},C_{BAL}^{(n)}+\Delta C_{BAL}\right]\right)-P_{TXL}\left(\left[R_{BAL}^{(n)},C_{BAL}^{(n)}\right]\right)\end{aligned} \tag{3.7}$$

Some standard solutions allow to improve the algorithm performance, integrating system preconditioning or using adaptive steps (e.g. based on *line-search algorithm*), but they give rise to a more complicated control system. In the designed system, the discrete domain of the variables suggests choosing a step size like in the *binary search method*

$$\boldsymbol{\gamma}^{(n)}=[\gamma_1^{(n)},\gamma_2^{(n)}]=[2^{B_1-n-2}\Delta R_{BAL},2^{B_2-n-2}\Delta C_{BAL}] \tag{3.8}$$

The initial balancing impedance value (i.e. iteration n=0) is equal to the middle point of the available range

$$Z_{BAL}^{(0)}=[R_{BAL}^{(0)},C_{BAL}^{(0)}]=[2^{B_1-1}\Delta R_{BAL},2^{B_2-1}\Delta C_{BAL}] \tag{3.9}$$

and the step size is one-fourth of the range. At every iteration the step size is automatically defined by the weight of the bit to set, from the MSB to the LSB. In this way, the number of iterations is fixed equal to B_1-*1*, set by the width of the digital words that control the balancing impedance. However, the gradient components estimation, as described in (3.7), introduces an uncertainly equal to ±1LSB on the optimal resistance and capacitance values. For this reason, it is possible to skip the last step, leaving unset the LSBs, whose values will be defined in the tracking phase (or fine search).

3.3.2 Tracking Phase

As introduced in Section 3.2, the interactions between the antenna and the external environment could result in a variation of the optimal

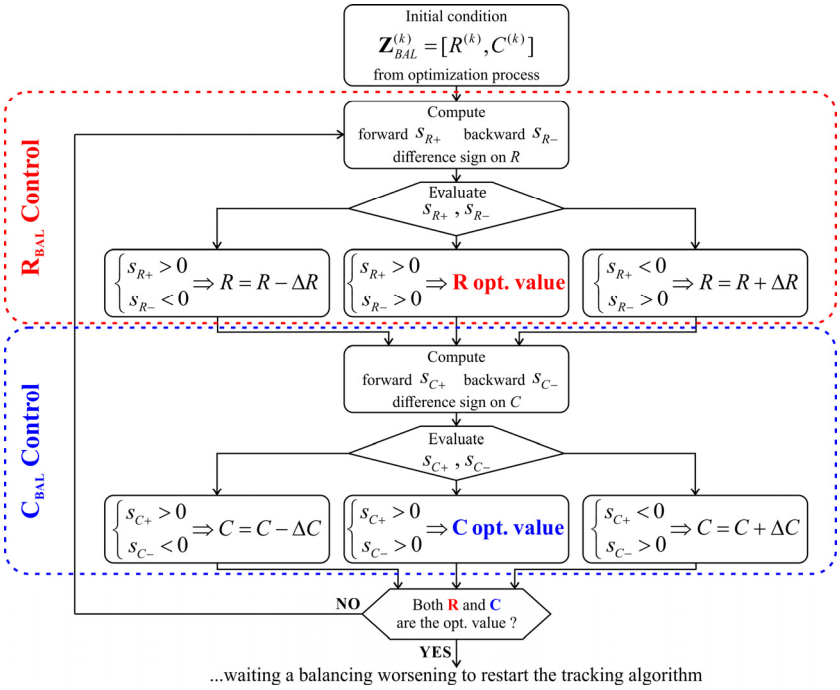

Figure 3.4: Flowchart of the tracking algorithm

balancing condition, worsening the TX-RX isolation level. Assuming these variations inherently much slower if compared with the settling time of the control system (e.g. a convergence time of ≈100us in a balancing variation time of ≈10ms), only a few LSBs should be tuned to follow these interferences. Reinitializing the optimization phase would allow to restore the balancing in a reasonable time, but it could lead to a temporary sudden drop in the $ISO_{TX\text{-}RX}$. Therefore, the purpose of the tracking phase is to keep the isolation level always high, with a real-time control of the matching condition. Figure 3.4 shows the tracking process flowchart: considering that it is usually activated after the coarse search (i.e. the optimization phase), the starting point is the result of the previous process. Similar to the optimization algorithm, the tracking exploits the gradient components sign to follow the drift of the optimum point, but here both forward s_+ and backward s_- difference are computed. Moreover, the updating step size is fixed and equal to the variables LSBs. These features allow to find the optimum impedance

value with the maximum precision, separately acting on the two variables in order to change their value as needed. It is worth noting that this fine search improves the overall robustness of the control system introducing a kind of redundancy degree; it allows to correct any random errors resulting, for instance, from a wrong estimation of the gradient components, that could occur during the optimization process. The only effect of these errors will be a tolerable increase of the convergence time. At the end of the process, when the optimal balancing is found, the control system continuously checks the TX leakage power at a lower rate. When the signal goes above a certain threshold, the tracking phase is activated again to restore the maximum isolation.

3.3.3 Error Probability and Monte Carlo Method

As previously explained, the control system finds the optimal value estimating the gradient components through real-time P_{TXL} measurement as reported in (3.2). This signal gives an approximation of the instantaneous transmitted power that couples to the receiver path. However, there are different noise sources which could compromise the signal estimation. Estimating the gradient as reported in (3.7), the noise on the measured signal determines a noise on the difference

$$\begin{aligned} &P_{TXL}(Z_{BAL}) = P'_{TXL}(Z_{BAL}) + n_P \qquad n_P = \mathrm{N}\left(0,\sigma_P^2\right) \\ &dif_R P_{TXL}(Z_{BAL}) = dif'_R P_{TXL}(Z_{BAL}) + n_d \qquad n_d = \mathrm{N}\left(0,\sigma_d^2\right) = \mathrm{N}\left(0,2\sigma_P^2\right) \end{aligned} \tag{3.10}$$

given by the sum of the noise-less signal and an additive white Gaussian noise (the signal $dif_R P_{TXL}(Z_{BAL})$ assumes a distribution $\mathrm{N}\left(\mu_d, 2\sigma_P^2\right)$). Reminding that the signal of interest is only the difference sign, a sufficient condition which allows to avoid an incorrect evaluation is

$$x = \frac{|n_d|}{\left|dif'_R P_{TXL}(Z_{BAL})\right|} < 1 \tag{3.11}$$

In the above expression the normalized error is reported, whose

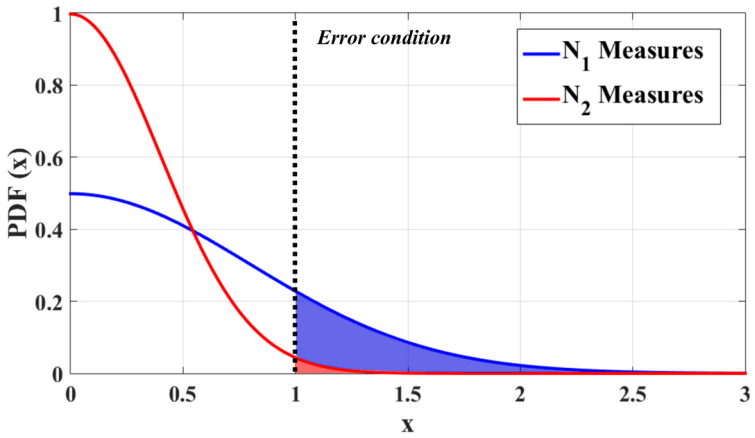

Figure 3.5: Probability density function of the normalized error x with different number of measurements (N2>N1)

probability density function *PDF(x)* is showed in Fig. 3.5. The filled area beyond the error condition x=1 defines the error probability, that can be computed as follows

$$P\left(n_d > dif'_R P_{TXL}(Z_{BAL})\right) = \frac{1}{2} erfc\left(\sqrt{dif'_R P_{TXL}(Z_{BAL})^2 / 2\sigma_P^2}\right) = \\ = \frac{1}{2} erfc\left(SNR_{dif}\right) \tag{3.12}$$

The probability to get a wrong estimation of the gradient components sign depends on the input SNR: the lower it is, the higher is the error probability. However, it is easy to improve the SNR in the digital domain taking multiple signal acquisitions, although this approach introduces a trade-off between measurement reliability and convergence time. It could be useful to define a dynamic system, which allows to adapt the number of measurements to keep the error probability below a tolerated value, without significantly compromising the overall control system performance. Assuming to perform N measurements of the signal $dif_R P_{TXL}(Z_{BAL})|_{t_i}$, the result is a sampling of a normally distributed population, from which an estimator η of its expected value is modeled. Its sample mean and sample variance are equal to

$$\eta = \frac{1}{N}\sum_{i=1}^{N} dif_R P_{TXL}(Z_{BAL})\Big|_{t_i}$$
$$\sigma_\eta^2 = \frac{1}{N}\sum_{i=1}^{N}\left(dif_R P_{TXL}(Z_{BAL})\Big|_{t_i} - \eta\right)^2 \quad (3.13)$$

With N small, this estimator shows a Student's t-distribution with *N-1* degree of freedom

$$t = \frac{\eta - \mu_d}{\frac{\sigma_\eta}{\sqrt{N}}} \quad (3.14)$$

Fixed a confidence level α, there is the $(1-\alpha)\cdot 100\%$ of probability that the relative error is

$$\left|\frac{t_\alpha \sigma_\eta}{\eta\sqrt{N}}\right| < 1 \quad (3.15)$$

where the value $t_\alpha = f(N,\alpha)$ is obtained from the Student's t-distribution. The proposed approach belongs to the general class of the so-called *Monte Carlo methods*: according to the input SNR, the system defines the number of measurement to meet the error condition with a certain confidence level, depending on the desired system robustness.

3.4 Performance Evaluation

This control system is designed to ensure enough TX-RX isolation without limiting the normal transceiver operations, reaching the desired specification ($T_{conv} \approx$ 100 µs) even with modulated signals. To verify the control system performance, a mixed-signal model (Fig. 3.1) was created in MatLab-Simulink environment with the given analog system and an equivalent model of a realistic Planar Inverted-F Antenna (*PIFA*) [15]. Progressively more complex and realistic cases will be assumed, from a simple noise-less tone to a 1024-QAM modulated signal, providing a solution which allows to make the system convergence time up to 2.5x faster than the previous solution [5], thus

enabling its operation for HT-based mobile transceivers.

3.4.1 Sine Wave TX Signal

As reported in (3.2), the measured signal is the instantaneous TX leakage power; for the preliminary considerations, a simple tone at baseband frequency f_{TX} is considered as transmitted signal (f_c is the carrier frequency)

$$V_{TX}(t) = A\cos\left(2\pi(f_c + f_{TX})t\right) \tag{3.16}$$

Considering the UMTS/FDD standard supported by the receiver under test, the carrier frequency is f_c = 2GHz and the baseband frequency is f_{TX} = 2.5 MHz. After the down-conversion the evaluated signal (3.2) becomes

$$P_{TXL}(Z_{BAL}) = A^2 Iso(Z_{BAL})^2 \tag{3.17}$$

that is the average transmitted power multiplied by the magnitude of the isolation level, a function of the HT balancing conditions (3.1). Assuming an ideal noise-less signal, the overall control system convergence time can be computed as follows

$$T_{conv} = (2 \cdot N_{opt.steps} + 3 \cdot N_{trk.steps}) \cdot N_{meas} \cdot T_{meas} \tag{3.18}$$

In the above equation, $N_{opt.steps}$ and $N_{trk.steps}$ are the number of steps in optimization and tracking phase respectively: $N_{opt.steps}$ is multiplied by 2 because in the optimization phase only the forward difference is computed and hence two measurements of the signal P_{TXL} are needed; indeed, $N_{trk.steps}$ is multiplied by 3 because in the tracking phase both forward and backward difference are used. N_{meas} is the number of signal evaluations and T_{meas} is the measurement time of P_{TXL}. Assuming a Nyquist sampling frequency (5 MHz), T_{meas} is equal to 200ns. Since at least two measurements are required to define sample mean and sample variance from (3.13), the ideal convergence time is 10.4 μs, that is far below the required one (e.g. ≈100 μs). Considering a more realistic case in which a noise, for instance generated by the receiver front end, is superimposed on the ideal signal (3.17)

$$P_{TXL}(Z_{BAL}) = A^2 Iso(Z_{BAL})^2 + n_P \tag{3.19}$$

this noise could lead to a wrong evaluation of the signal, as explained in the previous section. However, the proposed Monte Carlo approach (3.15) adapts the number of signal valuations N_{meas} according to the input SNR, ensuring the measurements reliability with a given confidence level. A minimum SNR_{dif} is needed to guarantee an acceptable convergence time. Considering a $T_{conv} < 100$ µs, from (3.18) it is easy to define the maximum number of signal evaluations $N_{meas} < 19$. Assuming an maximum error probability of 0.1%, from (3.15) the minimum required SNR is achieved

$$SNR_{dif} = \left|\frac{\eta}{\sigma_\eta}\right| > \frac{t_\alpha}{\sqrt{N}} \tag{3.20}$$

that is, in the described case, $SNR_{dif} > -3$dB ($T_{meas} = 200$ ns as in the previous case). The Monte Carlo method models an estimator for the gradient (i.e. *dif*) and hence the required *SNR* is defined on this signal. However, assuming that the noise is generated by the receiver chain and thus independent on the isolation level, the minimum SNR_{dif} is reached around the optimum value, where the signal P_{TXL} is minimized. Therefore, this parameter fixes required receiver sensitivity, as it will be explained in Section 3.5. Since the SNR is minimum around the optimum value of Z_{BAL}, the Monte Carlo method reduces the number of signal evaluations N_{meas} through the optimization process, resulting, from simulation, in an average convergence time $T_{conv} = 80$ µs with different optimal balancing configurations.

3.4.2 Modulated TX Signal

In order to control the HT balancing condition during the normal transmission operations, it is necessary to deal with a realistic transmitted signal, characterized by a certain digital modulation and bandwidth which depend on the standard specifications supported by the transceiver. As mentioned before, the designed control system is

tailored to an integrated duplexer receiver prototype compatible with the 3G standard, therefore the signal bandwidth is set to 5 MHz; regarding the signal modulation, the system will be tested in different cases. To limit the transmitted signal bandwidth, a Root Raised Cosine (RRC) with a roll-off factor of 0.2 is used as pulse shaping filter. At first, a QPSK signal is considered

$$V_{TX}(t) = A\cos\left(2\pi f_c t + (2n-1)\frac{\pi}{4}\right) \quad n = 1,2,3,4 \tag{3.21}$$

that should still give rise to a signal P_{TXL} like (3.17), that represents in this case the transmitted symbol power. Indeed, PSK modulations ideally show a constant average symbol power, corresponding to a PAPR equal to one. However, the RRC filter increases the signal PAPR, leading to a limited input SNR_{PTX}. In the previous section, with an ideal transmitted signal (3.16) (unlimited SNR_{PTX}), the corresponding TX leakage power (3.19) can be degraded by the receiver noise that is independent from the HT isolation level. But with a modulated signal, the finite transmitted signal/noise ratio SNR_{PTX} is related to the modulation, which will influence the SNR_{dif} and hence the system performance. With the control system explained so far, the average convergence time is T_{conv} = 117 µs with a QPSK signal and T_{conv} = 165 µs with an 8-PSK signal. Even though these values are higher than the desired convergence time, they still remain far below the balancing variation time (which is ≈10ms) and hence it would not be necessary to complicate the control system- If a TX signal with an amplitude modulation, for instance a 16-QAM signal, is considered

$$\begin{aligned} &V_{TX}(t) = A\left[\alpha_1 \cos\left(2\pi f_c t\right) - \alpha_2 \sin\left(2\pi f_c t\right)\right] \\ &\alpha_1 = \pm 1, \pm 2 \quad \alpha_2 = \pm 1, \pm 2 \end{aligned} \tag{3.22}$$

a sharp worsening of the control system performance is expected, due to the higher PAPR of the modulation technique. Indeed, the system simulation shows a T_{conv} = 350 µs, leading to a no longer negligible time. The results are even worse considering more complex modulation

schemes: the convergence time increases up to 388 and 441 μs with 64 and 1024-QAM respectively.

3.4.3 Control Algorithm Improvement

The control system shows its limits when a realistic modulated signal is considered. The aim is to find a solution to improve the control system performance without increasing its complexity. Using the same algorithm and sampling frequency, the only parameter that can be improved to reduce the convergence time is, from (3.18), the number of signal evaluation $N_{meas.}$ Since, from (3.20), N_{meas} depends on $SNR_{dif.}$, the relation between the SNR_{dif} and SNR_{PTX} will be determined. In order to simplify the following analysis, the isolation level (3.1) is equivalently expressed in terms of admittances

$$ISO_{TX-RX} = \left|\frac{Y_{ANT} - Y_{BAL}}{Y_{ANT} + Y_{BAL}}\right| = \left|\frac{(G_A - G_B) + j(B_A - B_B)}{(G_A + G_B) + j(B_A + B_B)}\right| \qquad (3.23)$$

$$Y_{ANT} = G_A + jB_A \qquad Y_{BAL} = G_B + jB_B$$

Considering that the signal of interest is the gradient, estimated through finite difference approximation, from (3.7) and (3.10) it can be expressed as follows:

$$\begin{aligned} &dif_G P_{TXL}(Y_{BAL}) = dif'_G P_{TXL}(Y_{BAL}) + n_d(Y_{BAL}) = \\ &= \left(P_{TXL}([G_B + \Delta G_B, B_B]) - P_{TXL}([G_B, B_B])\right) + n_d(Y_{BAL}) \end{aligned} \qquad (3.24)$$

where, for simplicity, only the difference on the conductance of the balancing admittance is taken into account. In this case, the noise is related to the transmitted signal and hence it is dependent on the HT response; however, the noise of the receiver chain is still present and degrades the SNR_{dif} around the optimum value. Since the effects related to this noise have been previously considered, at first approximation it will be neglected. Therefore, the SNR_{dif} is defined as

$$SNR_{dif} = \frac{\left| P_{TXL}\left(\left[G_B + \Delta G_B, B_B\right]\right) - P_{TXL}\left(\left[G_B, B_B\right]\right)\right|}{\sqrt{\sigma^2_{P_{TXL}\left(\left[G_B+\Delta G_B, B_B\right]\right)} + \sigma^2_{P_{TXL}\left(\left[G_B, B_B\right]\right)}}} \tag{3.25}$$

and, assuming that

$$\begin{aligned} P_{TXL}\left(\left[G_B, B_B\right]\right) &= ISO_{TX-RX}\left(\left[G_B, B_B\right]\right)^2 P_{TX} \\ \sigma^2_{P_{TXL}\left(\left[G_B, B_B\right]\right)} &= ISO_{TX-RX}\left(\left[G_B, B_B\right]\right)^4 \sigma^2_{P_{TX}} \\ SNR_{P_{TX}} &= \frac{P_{TX}}{\sigma_{P_{TX}}} \end{aligned} \tag{3.26}$$

after a few arithmetic steps the normalized SNR_{dif} is obtained

$$\frac{SNR_{dif}}{SNR_{P_{TX}}} = \left| \frac{\Delta G_B\left[\Delta G_B + \left(G_A - G_B\right)\right]}{\Delta G_B{}^2 + 2\left[\left(G_A - G_B\right)^2 + \left(B_A - B_B\right)^2 + \Delta G_B\left(G_B - G_A\right)\right]} \right| \tag{3.27}$$

In Fig. 3.6a the function (3.27) is validated through comparison with simulations, assuming a certain optimal configuration and considering $B_A = B_B$. Obviously, a slight difference between analytical model and simulation is expected, due to the HT response approximation but, in this analysis, it is not necessary to find an exact matching, but only try to understand the relationship $SNR_{dif} = f\left(SNR_{P_{TX}}\right)$ and to look for a solution to improve the control system performance. The maximum SNR_{dif} is obtained around the optimum point, where it is approximatively equal to the SNR_{PTX}. However, as the balancing conductance deviates from the optimum value, the SNR_{dif} sharply drops, giving rise to a higher number of measurements. Until now, as defined in (3.7) and (3.24), the difference is computed by switching a single LSB. Obviously, maximizing the precision, this is the best solution around the optimum point, where only a few LSBs of the balancing impedance have to be set. However, it is possible to increase the signal difference (i.e. the SNR_{dif}) switching between two farther points, reducing the convergence time during the optimization phase.

Introducing an integer adaptive factor K, the difference computation becomes

$$\begin{aligned} dif_G P_{TXL}\left(Y_{BAL}\right) &= dif'_G P_{TXL}\left(Y_{BAL}\right) + n_d = \\ &= \left(P_{TXL}\left(\left[G_B + K\cdot\Delta G_B, B_B\right]\right) - P_{TXL}\left(\left[G_B, B_B\right]\right)\right) + n_d \end{aligned} \tag{3.28}$$

and the normalized SNR_{dif} from (3.27) becomes

$$\frac{SNR_{dif}}{SNR_{P_{TX}}} = \left| \frac{K\cdot\Delta G_B\left[K\cdot\Delta G_B + \left(G_A - G_B\right)\right]}{\left(K\cdot\Delta G_B\right)^2 + 2\left[\left(G_A - G_B\right)^2 + \left(B_A - B_B\right)^2 + K\cdot\Delta G_B\left(G_B - G_A\right)\right]} \right| \tag{3.29}$$

This parameter can be chosen evaluating the TX leakage power: the higher is P_{TXL} (which means that the control system is far from the optimum point), the higher can be K. Obviously this factor has to be wisely chosen to reach a good compromise between convergence time and stability of the control system. For example, considering the available range, the parameter is set K={1 (near the optimum), 4, 8, 16 (far from the optimum)} for the balancing resistances and K= {1, 2, 4} for the balancing capacitances. Figure 3.6b shows the difference of the normalized SNR_{dif} between fixed and variable K approach: far from the optimum point a higher K determines an improvement of more than 10dB, leading to a reduced number of signal measurements; near the optimum point, where K is smaller, the two curves converge, recovering the required precision. Finally, to prove the advantages introduced by this new method, the improved control algorithm is tested with the same modulated signal previously employed. Table 3.2 summarizes the obtained results; with a fixed step K=1 (as in [5]), the convergence time rises up to 441 μs with high PAPR modulation schemes (1024-QAM). The adaptive step, which does not complicate the control algorithm, improves the convergence time, that becomes up to x2.5 smaller considering QAM modulation schemes. Although the obtained results make the system able to follow the external environment variations,

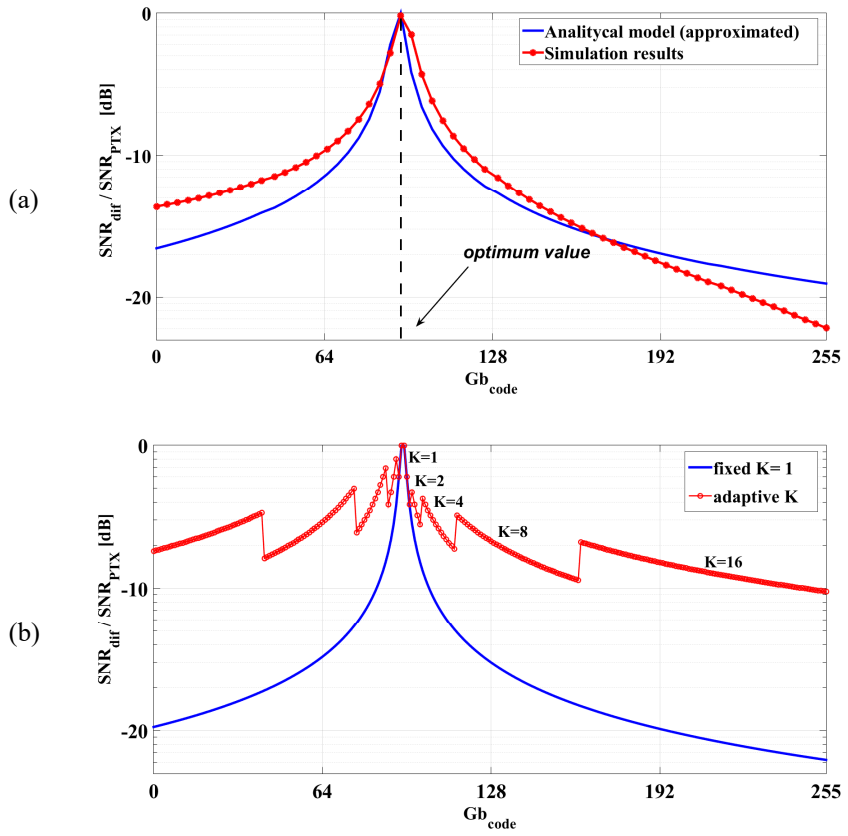

Figure 3.6: Normalized SNR_{dif} with fixed optimal configuration, (a) comparison between analytical model (3.27) and simulation results, (b) comparison between fixed and adaptive step K, considering the analytical model (3.29)

advanced mobile standards (e.g. LTE and beyond) may impose more stringent settling requirements. Several improvements may be introduced to further shorten the convergence time, with a slight increase in complexity and power dissipation of the control system. A possible solution would be the use of an oversampling factor to reduce the single measurement time and hence the whole process duration. Another solution consists of normalizing the measured leakage power to the known signal generated by the local digital transmitter: this solution, limiting the dependence on the transmitted symbol, would allow to reduce the PAPR of the measured signal, thus increasing the SNR_{PTX}. All these enhancements make the proposed system suitable to

TABLE 3.2
CONTROL SYSTEM CONVERGENCE TIME WITH DIFFERENT TX SIGNALS

TX Signal	**Average Convergence Time [μs]**	
Ideal (noise-less tone)	10.4	
Tone + noise	80	
	Fixed K=1 [5]	**Adaptive K This Work**
QPSK	117	**91**
8-PSK	165	**102**
16-QAM	350	**135**
64-QAM	388	**148**
1024-QAM	441	**179**

realize a background control with high PAPR transmitted signals as well.

3.5 Hardware Implementation

The proposed circuit is designed to control a HT-based receiver which supports FDD standards; therefore, an auxiliary path with relaxed performance is needed to sense the TX leakage for the digital control network, allowing the balancing control in background. Therefore, the goal is to minimize the overhead introduced (mainly area and power) by this auxiliary path. Figure 3.7 shows the schematic of the complete system with the auxiliary receiver tuned at the TX frequency. The calibration of the hybrid transformer needs to be activated only when the transmitted power is relatively large, e.g. within a range of 50dB from the maximum transmitted power. Hence, for the 3G system under consideration, the control loop must be able to operate with an antenna referred TX power level anywhere from TX_{max}=+24 dBm to TX_{min}=-26 dBm. To relax the auxiliary receiver requirements, a passive variable attenuator before the auxiliary path is required, lowering the signal level to be detected and compressing the dynamic

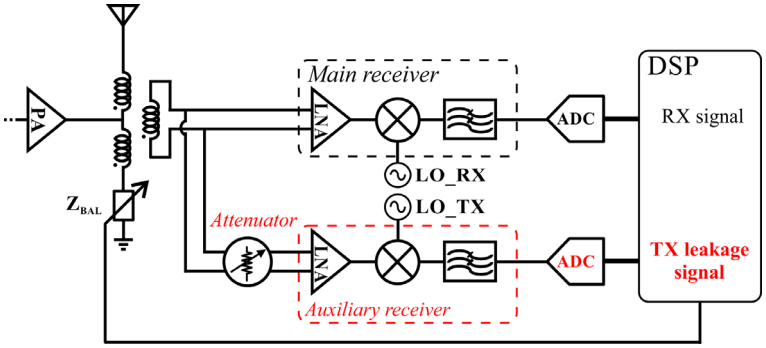

Figure 3.7: Auxiliary path for FDD standard applications

range. As an example, a reduction of the signal range by 30 dB could be obtained exploiting a simple attenuator with three different levels, $Att = \{20,30,50\}$ dB (Fig. 3.8 depicts the desired transfer function). This solution allows to bring the auxiliary input range to $Aux_{max} = -26$ dBm, $Aux_{min} = -46$ dBm. Moreover, from the auxiliary path point of view, the hybrid transformer acts as a variable attenuator, expanding the signal range to be covered (in this system, at least by 45 dB). As a result, the required sensitivity, 1-dB compression point and NF of the auxiliary receiver are, respectively, $P_{sens} < -91$ dBm, $P_{1dB} > -26$ dBm and, considering the desired *SNR* computed in Section 3.4.1, a NF < 18 dB. As an example, the receiver in [20] meets these requirements with only 0.6 mW of power. Two ADCs, placed at the end of the down-conversion chain, provide the input signals *I* and *Q* to the digital circuit, in order to estimate the P_{TXL} as reported in (3.2). As already explained,

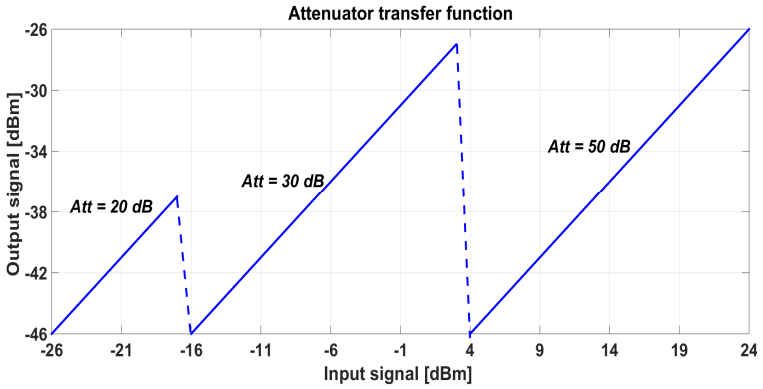

Figure 3.8: RF attenuator function vs TX power level

the ADCs sampling frequency is related to the receiver specifications, which supports (UMTS/FDD standard in this architecture); after down-conversion the two components *I* and *Q* have 2.5 MHz of bandwidth and hence the minimum sampling frequency is 5 MHz. The required ADC resolution depends on the dynamic range of the measured leakage signal. The worst case unbalancing conditions determine the maximum signal level, whereas the balancing impedance resolution sets the minimum signal to be detected. Therefore, the ADC dynamic range is computed as follows

$$DR \propto \frac{\max\left(P_{TXL}\right)}{\min\left(\nabla P_{TXL}\right)} \propto \frac{\max\left(ISO_{TX-RX}{}^{2}\right)}{\min\left(\nabla ISO_{TX-RX}{}^{2}\right)} \tag{3.30}$$

Considering range and resolution of the balancing impedance used in the proposed system, the required dynamic range is approximately 8 bits. Finally, an efficient hardware implementation of the proposed control system has been carried out, minimizing as much as possible the required area and power. The digital elaboration is realized in fixed-point arithmetic, with a wise data sizing through the processing chain to avoid data overflow condition and to minimize the quantization error in order to not compromise the final result. Figure 3.9 shows a simplified block diagram of the proposed digital circuit, where three fundamental sub-block can be individuate: the difference estimation, the Monte Carlo method and a Finite State Machine (FSM) that controls the balancing impedance. This FSM deals with the switching of resistance and capacitance to properly compute the differences used to estimate the gradient components and updating the balancing impedance through the expected steps in optimization and tracking phase. The first block (i.e. the difference estimation) receives as input the sampled signals I and Q from the ADCs, and hence it works at the sampling frequency, measuring the instantaneous TX leakage power as reported in (3.2). The adder and the shift register computes the signal *dif* that estimates the gradient component, clearly assuming that between the two P_{TXL} measurements the balancing impedance is properly switched by the FSM. It is worth to note that the frequency of

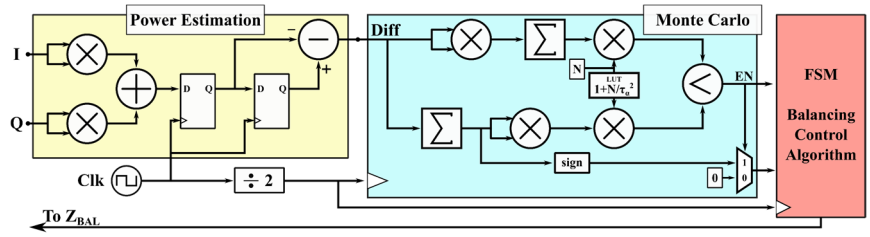

Figure 3.9: Block diagram of the proposed digital control circuit

the signal *dif* is halved, compared to the P_{TXL} frequency, for the way in which it is computed. Therefore, the output of the first block will be the difference estimation *dif*, which represents the input of the Monte Carlo block. Here, the proposed method is implemented to verify the condition (3.15), but the expression should be make more suitable for an equivalent digital implementation. The expression (3.15) can be equivalently written as

$$t_\alpha{}^2 \sigma_\eta{}^2 < \eta^2 N \tag{3.31}$$

and, from (3.13), the variance can be expanded as follows

$$\sigma_\eta{}^2 = \frac{1}{N}\sum_{i=1}^{N} dif\big|_{t_i}{}^2 - \left(\frac{1}{N}\sum_{i=1}^{N} dif\big|_{t_i}\right)^2 = \frac{1}{N}\sum_{i=1}^{N} dif\big|_{t_i}{}^2 - \eta^2 \tag{3.32}$$

getting, after a few steps, the inequality (3.31) expressed as

$$N\sum_{i=1}^{N} dif\big|_{t_i}{}^2 < \left(\sum_{i=1}^{N} dif\big|_{t_i}\right)^2 \left(1+\frac{N}{t_\alpha{}^2}\right) \tag{3.33}$$

The term $\left(1+N/t_\alpha{}^2\right)$ can be easily computed by using a small lookup-table (LUT) whose results, assuming a fixed confidence level α, only depends on N (i.e. the number of measurements of *dif*). The Monte Carlo block generates two outputs: the enable signal *EN* and the sign of the difference *sgn.* When the condition (3.33) is verified, the enable is high, and the signal *sgn* is propagated to the FSM. This last block properly updates the balancing impedance toward the optimum point following the steps as defined by the control algorithms. The

TABLE 3.3
REQUIREMENTS OF THE PROPOSED DIGITAL CONTROL SYSTEM

Digital circuit synthesis report	
Technology	40 nm CMOS
Frequency	5 MHz
Cell Area	7288 μm^2
Power	19.13 μW

proposed circuit has been synthesized in 40nm to verify its requirements, reported in Tab. 3.3.

3.6 Experimental Measurements

A photograph of the measurement setup is shown in Fig. 3.10: the RX-HT prototype chip [2] is bonded on a Printed Circuit Board (PCB) and it is biased through a National Instruments CRio-9014; a HP ESG-4000A Signal Generator provides the RX clock and a R&S SMU 200A is used to generate the modulated transmitted signal directly fed into the TX port; the PIFA prototype [8] is connected to the antenna port. Finally, the control algorithm is implemented on a Cyclone IV EP4CE115F29C7 Altera FPGA and an Altera Data Conversion Card with two configurable ADCs provides the I and Q digital signals to the digital processing. The sampling frequency is set to 5 MHz (Nyquist sampling frequency) and the data resolution is 8 bits (the minimum required). The processed data are then acquired from the FPGA through the SignalTap II Logic Analyzer Tool of Quartus. The measured ISO_{TX-RX} as a function of the balancing impedance using the PIFA [8] is shown in Fig. 3.11: the best approximation of the antenna impedance at the transmitted signal frequency ensures more than 60 dB peak isolation. To validate the designed control system, the same cases verified in Section 3.4 are considered: the sine wave and the modulated signal. However, considering that some pipeline stages are used on the dataflow of the digital circuit to avoid synchronization problems, an

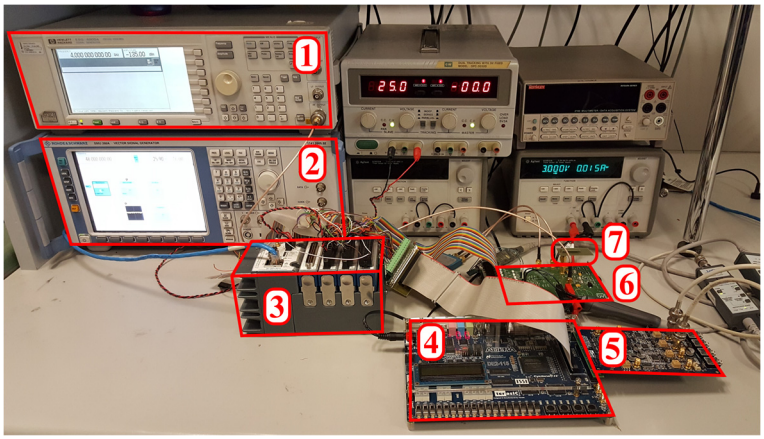

Figure 3.10: Measurement setup, RX clock generator (1); vector signal generator (2); NI CRio-9014 (3); Altera FPGA board (4); ADCs board (5); RX+HT chip prototype board (6); PIFA prototype (7)

overhead is introduced on the convergence time with respect to the simulated value (reported in Tab. 3.2). With a simple tone, the convergence time is limited by the receiver noise but, in this application, the receiver front-end [2] used to validate the control system has oversized specifications (as demonstrated in Section 3.5). Figure 3.11 shows the measured $ISO_{TX\text{-}RX}$ transient during the optimization process with a sinusoidal transmitted signal; the optimal configuration is found within ≈50 µs. As explained, this result is related to the measurement time (200 ns) and to the signal SNR (≈2.5 dB in this measurement setup) around the optimal Z_{BAL}. The expected

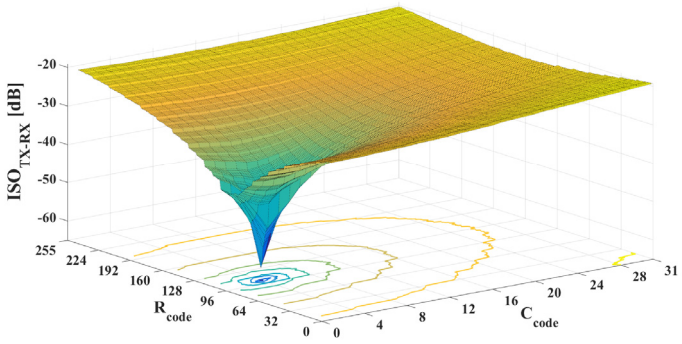

Figure 3.11: $ISO_{TX\text{-}RX}$ as a function of the balancing impedance, experimentally measured on the available receiver [2] using the PIFA [8]

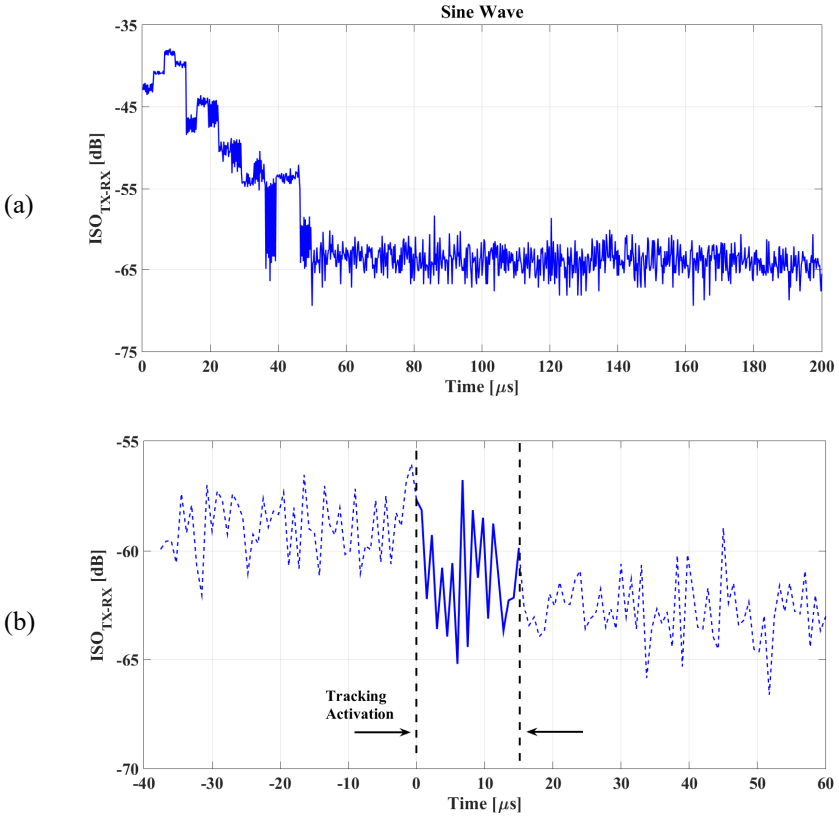

Figure 3.12: Measured $ISO_{TX\text{-}RX}$ transient during (a) optimization and (b) tracking phase, with a sinusoidal transmitted signal

convergence time from (3.20) should be ≈65 μs but, through the Monte Carlo approach which adapts the measurement time according to the effective input SNR, faster convergence is normally expected. To verify the operations performed during the tracking phase, the optimal balancing condition is slightly changed, shifting the transmitted signal by a few MHz. This operation allows to mimic the effect of antenna-environment interactions. As shown in Fig. 3.12b, after a few iterations, the optimal $ISO_{TX\text{-}RX}$ is restored. Finally, the system performance with different modulated signals has been verified, exploiting the improved algorithm version with adaptive step proposed in Section 3.4.3. Figure 3.13 shows the $ISO_{TX\text{-}RX}$ time waveform with a 16-QAM TX signal: the optimum value is reached after ≈150 μs. In order to be consistent with the rest of the work, the optimization process is considered completed

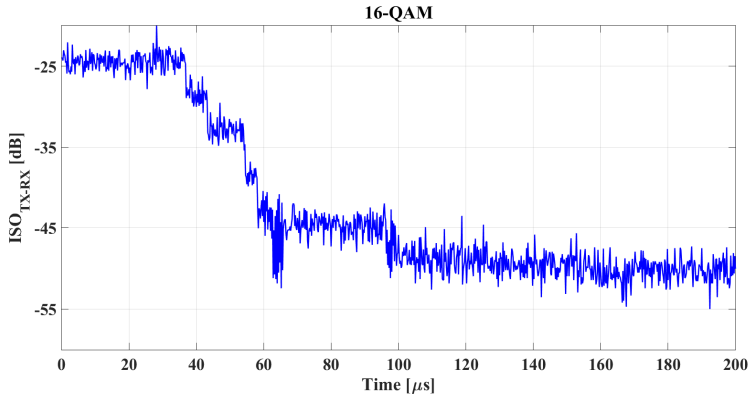

Figure 3.13: Measured $ISO_{TX\text{-}RX}$ transient with a 16-QAM transmitted signal

when the optimal value is found. However, ≈100 μs are enough to ensure more than 45 dB of isolation. Comparing the $ISO_{TX\text{-}RX}$ time waveform with a TX sine wave (Fig. 3.12.a) and a modulated TX signal (Fig. 3.13), the main difference is observed when the control system is far from the optimum point: with the sine wave, the low number of measurement is ensured by the high SNR, that shrinks down closer to the desired point; instead, with the modulated signal, due to the high PAPR, the SNR is low also far from the optimum point, worsening the convergence time. In Tab. 3.4 the average convergence time obtained in different balancing configurations with modulated signals are reported: the comparison with the simulation results shows that the hardware implementation of the control system preserves the desired performance, with a slight overhead due to the pipeline stages of the digital circuit. It is worth to note that the maximum isolation level (≈60dB assumed so far) is actually reached at only one frequency, due

TABLE 3.4
MEASURED CONVERGENCE TIME WITH DIFFERENT MODULATION SCHEMES

Modulation scheme	**Average Convergence Time [μs]**	
	Simulation	**Measurement**
QPSK	91	**105**
8-PSK	102	**127**
16-QAM	135	**153**

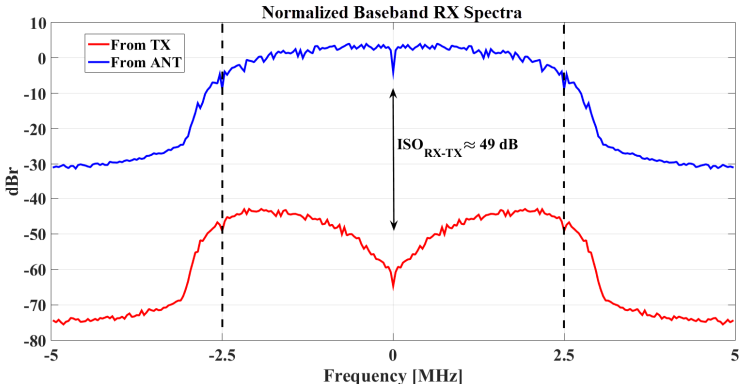

Figure 3.14: Measured baseband spectra of 5 MHz modulated signals at the HT antenna and TX port, with the PIFA [8]

to the antenna impedance frequency variations. Therefore, with a modulated signal, the optimal ISO_{TX-RX} is obtained when the $Z_{ANT} \approx Z_{BAL}$ at the TX carrier frequency (i.e. at the middle point of the signal bandwidth). Figure 15 shows the normalized baseband spectra of the signals at the HT antenna and TX port (P_{TXport} = 10dBm, $P_{ANTport}$ = -25dBm). The control system is able to find the balancing impedance value closer to the TX carrier frequency that maximizes $ISO_{TX-RX} \approx$49 dB over 5 MHz bandwidth.

Conclusion

In this thesis some of the problems that arise from the lack of SAW and Duplexer filters have been addressed. Chapter 2 dealt with the sensitivity degradation of a diversity receiver corrupted by the broadband Tx noise. An auxiliary receiver provides a baseband copy of the Tx noise in Rx band to an adaptive digital equalizer, which matches in real-time the antenna coupling effects and reduces the transmitted noise of about 29dB over 20MHz of bandwidth. This solution, validated by experimental measurements, restores the diversity receiver sensitivity, ensuring only 1.1 dB of NF degradation, and an equivalent -171 dBc/Hz noise-to-carrier ratio at 1 GHz. In Chapter 3 a low-power low-area digital control system tailored to a hybrid transformer-based receiver has been demonstrated. The synthesis in 40nm CMOS technology proves the feasibility of this solution, with a required area of 7288 μm^2 and a power consumption lower than 20 μW. The optimization process is completed in an acceptable time even when modulated signals are transmitted, whereas the tracking process allows to keep at all times the desired isolation level. The experimental results, obtained through FPGA implementation, are in good agreement with the formulated theory. The proposed system is an attractive solution even for future full-duplex architectures, enabling to maximize the TX-RX isolation level without interfering with the normal transceiver operations.

Bibliography

[1] B. Razavi, “RF Microelectronics,” 2nd Edition, Prentice-Hall Press, Upper Saddle River, NJ, USA, 2011.

[2] M. Ramella, I. Fabiano, D. Manstretta, and R. Castello, “A 1.7-2.1GHz +23dBm TX Power Compatible Blocker Tolerant FDD Receiver with Integrated Duplexer in 28nm CMOS”, *2015 IEEE Asian Solid-State Circuits Conference (A-SSCC)*, Xiamen, 2015, pp. 1-4.

[3] E. Kargaran, S. Tijani, G. Pini, D. Manstretta and R. Castello, "Low power wideband receiver with RF Self-Interference Cancellation for Full-Duplex and FDD wireless Diversity," *2017 IEEE Radio Frequency Integrated Circuits Symposium (RFIC)*, Honolulu, HI, 2017, pp. 348-351.

[4] D. Montanari, D. Manstretta, R. Castello, G. Castellano, “A 0.7-2 GHz Auxiliary Receiver with Enhanced Compression for SAW-less FDD,” presented at *ESSCIRC 2017 – 43rd European Solid State Circuits Conference (ESSCIRC)*, Leuven, Belgium, 2017.

[5] G. Castellano, D. De Caro, A. G. M. Strollo and D. Manstretta, "A low power control system for real-time tuning of a hybrid transformer-based receiver", 2016 *IEEE International Conference on Electronics, Circuits and Systems (ICECS)*, Monte Carlo, 2016, pp. 328-331.

[6] B. Hershberg, B. van Liempd, X. Zhang, P. Wambacq and J. Craninckx, "A dual-frequency 0.7-to-1GHz balance network for electrical balance duplexers," 2016 IEEE International Solid-State Circuits Conference (ISSCC), San Francisco, CA, 2016, pp. 356-357.

[7] E. Roverato et al., "13.4 All-digital RF transmitter in 28nm CMOS with programmable RX-band noise shaping," 2017 IEEE International Solid-State Circuits Conference (ISSCC), San Francisco, CA, 2017, pp. 222-223.

[8] D. Montanari, L. Silvestri, M. Bozzi and D. Manstretta, "Antenna coupling and self-interference cancellation bandwidth in SAW-less diversity receivers," *2016 46th European Microwave Conference (EuMC)*, London, 2016, pp. 731-734.

[9] B. Widrow, J. McCool and M. Ball, "The complex LMS algorithm," in *Proceedings of the IEEE*, vol. 63, no. 4, pp. 719-720, April 1975.

[10] S. Haykin, “Adaptive Filter Theory,” 3rd Edition, Prentice-Hall, Inc. Upper Saddle River, NJ, USA, 1996.

[11] J. G. Proakis, “Digital Communications,” 4th Edition, McGraw-Hill, New York, 2001.

[12] L. Laughlin, M. Beach, K. Morris, and J. L. Haine, “Electrical balance duplexing for small form factor realization of in-band full duplex”, IEEE Commun. Mag., vol. 53, no. 5, pp. 102–110, May 2015.

[13] S. Ramakrishnan, *et al.*, "A 65nm CMOS transceiver with integrated active cancellation supporting FDD from 1GHz to 1.8GHz at +12.6dBm TX power leakage," *2016 IEEE Symposium on VLSI Circuits (VLSI-Circuits)*, Honolulu, HI, USA, 2016.

[14] H. Yüksel, *et al.*, "A Wideband Fully Integrated Software-Defined Transceiver for FDD and TDD Operation," *in IEEE Journal of Solid-State Circuits* , vol. 52, no.5, May 2017.

[15] S. H. Abdelhalem, *et al.*, “Tunable CMOS Integrated Duplexer with Antenna Impedance Tracking and High Isolation in the Transmit and Receive Bands”, *IEEE Trans. on MTT*, pp. 2092–2104, Sep 2014.

[16] M. Mikhemar, H. Darabi and A. A. Abidi, "A Multiband RF Antenna Duplexer on CMOS: Design and Performance," *IEEE Journal of Solid-State Circuits*, vol. 48, no. 9, pp. 2067-2077, Sept. 2013.

[17] M.Mikhael, B. van Liempd, J. Craninckx, R. Guindi, and B. Debaillie, “A full-duplex transceiver prototype with in-system automated tuning of the RF self-interference cancellation”, *Proc. 1st Int. Conf. 5G Ubiquitous Connect.*, pp. 110–115, 2014.

[18] L. Laughlin, *et al.*, "Passive and Active Electrical Balance Duplexers," *IEEE Transactions on Circuits and Systems II: Express Briefs*, vol. 63, no. 1, pp. 94-98, Jan. 2016.

[19] S.H. Abdelhalem, P.S. Gudem, L.E. Larson, “Hybrid Transformer-Based Tunable Differential Duplexer in a 90-nm CMOS Process”, *IEEE Trans. on MTT*, pp. 1316-1326, Mar 2013.

[20] A. Selvakumar, M. Zargham and A. Liscidini, “Sub-mW Current Re-Use Receiver Front-End for Wireless Sensor Network Applications”, in *IEEE JSSC*, vol. 50, no. 12, pp. 2965-2974, Dec. 2015.

[21] Avriel, Mordecai, “Nonlinear Programming: Analysis and Methods”, Dover Publishing, 2003.